Draft version July 24, 2025
Typeset using LaTeX **twocolumn** style in AASTeX7

Beyond the Dot: an LRD-like nucleus at the Heart of an IR-Bright Galaxy and its implications for high-redshift LRDs

Pierluigi Rinaldi,[1] George H. Rieke,[1] Zihao Wu,[2] Carys J. E. Gilbert,[3] Fabio Pacucci,[2,4] Luigi Barchiesi,[3,5,6] Stacey Alberts,[7,1] Stefano Carniani,[8] Andrew J. Bunker,[9] Rachana Bhatawdekar,[10] Francesco D'Eugenio,[11,12] Zhiyuan Ji,[1] Benjamin D. Johnson,[13] Kevin Hainline,[1] Vasily Kokorev,[14] Nimisha Kumari,[7] Edoardo Iani,[15] Jianwei Lyu,[1] Roberto Maiolino,[11,12,16] Eleonora Parlanti,[8] Brant E. Robertson,[17] Yang Sun,[1] Cristian Vignali,[18,19] Christina C. Williams,[20] Christopher N. A. Willmer,[1] and Yongda Zhu[1]

[1] *Steward Observatory, University of Arizona, 933 North Cherry Avenue, Tucson, AZ 85721, USA*
[2] *Center for Astrophysics | Harvard & Smithsonian, 60 Garden St., Cambridge MA 02138 USA*
[3] *Department of Astronomy, University of Cape Town, Private Bag X3, Rondebosch 7701, South Africa*
[4] *Black Hole Initiative, Harvard University, 20 Garden St, Cambridge, MA 02138, USA*
[5] *Inter-University Institute for Data Intensive Astronomy, University of Cape Town, Private Bag X3, Rondebosch 7701, South Africa*
[6] *INAF–Istituto di Radioastronomia, Via Piero Gobetti 101, I-40129 Bologna, Italy*
[7] *AURA for the European Space Agency (ESA), Space Telescope Science Institute, 3700 San Martin Dr., Baltimore, MD 21218, USA*
[8] *Scuola Normale Superiore, Piazza dei Cavalieri 7, I-56126 Pisa, Italy*
[9] *Department of Physics, University of Oxford, Denys Wilkinson Building, Keble Road, Oxford OX1 3RH, UK*
[10] *European Space Agency (ESA), European Space Astronomy Centre (ESAC), Camino Bajo del Castillo s/n, 28692 Villanueva de la Cañada, Madrid, Spain*
[11] *Kavli Institute for Cosmology, University of Cambridge, Madingley Road, Cambridge, CB3 0HA, UK*
[12] *Cavendish Laboratory, University of Cambridge, 19 JJ Thomson Avenue, Cambridge, CB3 0HE, UK*
[13] *Center for Astrophysics | Harvard & Smithsonian, 60 Garden St., Cambridge MA 02138 USA*
[14] *Department of Astronomy, The University of Texas at Austin, Austin, TX 78712, USA*
[15] *Institute of Science and Technology Austria (ISTA), Am Campus 1, 3400 Klosterneuburg, Austria*
[16] *Department of Physics and Astronomy, University College London, Gower Street, London WC1E 6BT, UK*
[17] *Department of Astronomy and Astrophysics, University of California, Santa Cruz, 1156 High Street, Santa Cruz, CA 95064, USA*
[18] *Dipartimento di Fisica e Astronomia, Alma Mater Studiorum, Università degli Studi di Bologna, Via Gobetti 93/2, 40129 Bologna, Italy*
[19] *INAF–Osservatorio di Astrofisica e Scienza dello Spazio di Bologna, Via Gobetti 93/3, 40129 Bologna, Italy*
[20] *NSF National Optical-Infrared Astronomy Research Laboratory, 950 North Cherry Avenue, Tucson, AZ 85719, USA*

ABSTRACT

Little Red Dots (LRDs) are compact, red sources discovered by JWST at high redshift ($z \gtrsim 4$), marked by distinctive "V-shaped" spectral energy distributions (SEDs) and often interpreted as rapidly accreting AGNs. Their evolution remains unclear, as identifying counterparts at lower redshifts is challenging. We present WISEA J123635.56+621424.2 (here dubbed *the Saguaro*), at $z = 2.0145$ galaxy in GOODS-North, as a possible analog of high-redshift LRDs and a potential missing link in their evolutionary path toward lower-redshift systems. It features a compact LRD-like nucleus surrounded by a face-on spiral host. Its connection to LRDs includes that: (1) its nuclear spectrum shows a clear "V-shaped" SED; and (2) when redshifted to $z = 7$, surface brightness dimming makes the host undetectable, thus mimicking an LRD. This suggests that high-redshift LRDs may be embedded in extended hosts. To test this, we stack rest-frame UV images of 99 photometrically selected LRDs, revealing faint, diffuse emission. Stacking in redshift bins reveals mild radial growth, consistent with the expected galaxy size evolution. A simple analytic model confirms that surface brightness dimming alone can explain their compact appearance. Lastly, we show that *the Saguaro* is not unique by describing similar objects from the literature at $z \lesssim 3.5$. Taken together, our results support a scenario in which LRDs may not be a distinct population, but could be the visible nuclei of galaxies undergoing a short-lived, AGN-dominated evolutionary phase, with their compact, red appearance driven largely by observational biases.

Email: prinaldi@arizona.edu

Keywords: Active galactic nuclei (16); High-redshift galaxies (734); Galaxy evolution (594); Near in-frared astronomy (1093); AGN host galaxies (2017); Galaxy formation (595); Photoionization (2060); Spectral energy distribution (2129); Infrared astronomy (786); Galaxies (573); Infrared photometry (792)

1. INTRODUCTION

One of the goals in building JWST (J. P. Gardner et al. 2023) was to see far enough back in time that fundamental differences would be apparent in galaxies and active galactic nuclei (AGNs). Pre-JWST, although number counts of nearly all classes of objects were found to evolve strongly, the properties of individual objects seemed familiar in comparison with relatively nearby analogs. This implied that we were not yet reaching far enough to witness their birth and earliest stages of evolution.

JWST has now extended our studies well into the infrared and thus allowed us to probe a much broader range of AGN properties in the early Universe, including greater distances and broad spectral behavior.

For example, Seyfert-luminosity AGNs at $z > 4$ appear to host significantly overmassive supermassive black holes (SMBHs; e.g., Y. Harikane et al. 2023; R. Maiolino et al. 2023; F. Pacucci et al. 2023). Even more interestingly, JWST has unveiled an apparently new class of compact, red sources, commonly referred to as "Little Red Dots" (LRDs; e.g., L. J. Furtak et al. 2023; M. Killi et al. 2023; V. Kokorev et al. 2023; H. Übler et al. 2023; H. B. Akins et al. 2024; G. Barro et al. 2024a; J. E. Greene et al. 2024; D. D. Kocevski et al. 2024; V. Kokorev et al. 2024; J. Matthee et al. 2024; K. N. Hainline et al. 2024; P. G. Pérez-González et al. 2024; P. Rinaldi et al. 2024; C. C. Williams et al. 2024). These sources have attracted significant attention due to their abundance at $z \approx 4$–9. Many have direct evidence for the presence of AGNs, but host galaxies have been elusive (C.-H. Chen et al. 2025b). It is now believed that LRDs represent an important stage in AGN formation and evolution that was not known prior to JWST.

Observations have now established that LRDs exhibit distinctive SEDs, marked by a characteristic "V-shape": a flat, blue UV continuum that transitions sharply into a steep red optical-to-near-infrared slope. This SED turnover typically occurs around rest-frame 3600 Å (e.g., D. J. Setton et al. 2024). Interestingly, LRDs remain unresolved in the longest-wavelength NIRCam broadband (F444W), which suffers from lower spatial resolution (compared to the shorter-wavelength NIRCam bands). In contrast, short-wavelength NIRCam observations reveal that LRDs often exhibit a complex morphology (P. Rinaldi et al. 2024). When spectroscopy is available (e.g., NIRSpec or NIRCam/WFSS), broad Balmer lines with FWHM $\gtrsim 1000$ km s^{-1} are often detected, indicating AGNs powered by SMBHs with $M_\bullet \approx 10^{6-8}\ M_\odot$ (e.g., L. J. Furtak et al. 2023; M. Killi et al. 2023; V. Kokorev et al. 2023; F. Pacucci et al. 2023; J. Matthee et al. 2024; P. Rinaldi et al. 2024; J. Zhang et al. 2025). Furthermore, they are typically X-ray and radio faint (T. T. Ananna et al. 2024; G. Mazzolari et al. 2024; M. Yue et al. 2024; R. Maiolino et al. 2025; K. Perger et al. 2025).

Despite the large number of studies published since their discovery, LRDs remain elusive, and understanding their true nature still requires a multi-faceted approach. This paper addresses two fundamental questions: *what do these sources evolve into as the Universe matures?* and *do they emerge from ordinary galaxies, or are they born in fundamentally different environments?* Answering the first question is difficult as observations have shown that the number density of LRDs drops dramatically toward lower redshifts (D. D. Kocevski et al. 2024; V. Kokorev et al. 2024; Y. Ma et al. 2025). They may evolve into a variety of objects with related, but different characteristics, making identifications ambiguous.

The scarcity of LRDs at $z < 4$ also makes it difficult to answer the second question, as it limits our ability to study analogs in a regime where host galaxies would be more easily detected and used to inform the nature of their high-redshift counterparts.

In this paper, we will look at relatively low redshift analogs both to learn more about the possible family tree of canonical LRDs and to see if they give hints on how to interpret the observations at higher redshift. Some analogs at $z \lesssim 3-4$ have been identified, showing similarities with LRDs (e.g., I. Juodžbalis et al. 2024; R. Lin et al. 2024; M. Stepney et al. 2024; F. Loiacono et al. 2025; A. de Graaff et al. 2025a; Y. Ma et al. 2025). Nonetheless, these discoveries are rare and no clear picture has emerged. Fortunately, rapid progress is being made to find larger samples. Using a thorough search of the SDSS database, X. Lin et al. (2025) have identified three objects at $z \approx 0.1$ that match LRD properties closely (also Ji et al., in prep.). This is an important advance, but emphasizes how rare local close matches to canonical LRDs are. J.-B. Billand et al. (2025) have explored the possibility that LRDs evolve by forming envelopes of young extended galaxies. To explore this

possibility, they selected from a much larger sample of 55 red galaxies at $z_{med} = 3.6 \pm 1.1$ with such envelopes and derived their properties, concluding that these objects likely represent the next evolutionary step. However, their study does not explore alternative pathways: an important limitation, given the broad range of properties observed in canonical LRDs at high redshifts (e.g., P. G. Pérez-González et al. 2024). That is, the evolutionary picture at $z \lesssim 3$ remains unclear.

This paper discusses the missing link between these two studies, i.e. objects potentially related to LRDs at redshifts between 0.2 and 3.5. Many of the proposed LRD analogs have been identified through JWST observations. It is important to note that, prior to JWST, the *Spitzer* mission (R. D. Gehrz et al. 2007) identified a variety of extragalactic sources in this redshift regime, the so-called Blue-excess Dust-obscured Galaxies (Blue HotDOG; R. J. Assef et al. 2016; A. Noboriguchi et al. 2022), which exhibit SEDs remarkably similar to those of LRDs as highlighted by A. Noboriguchi et al. (2023). Thus, they are a second good hunting ground for LRD analogs.

As part of the ongoing effort to bridge this gap, we have studied in detail WISEA J123635.56+621424.2 (here dubbed as *the Saguaro*[21]), originally brought to prominence with *Spitzer* as an infrared bright, optically faint galaxy (e.g., J. L. Donley et al. 2010). It is a well-studied object at $z = 2.0145$, located in GOODS-North (GOODS-N). It has an obscured AGN and a compact core in imaging from the *Hubble* Space Telescope (HST). Furthermore, its X-ray flux is very faint, indicating that it is Compton Thick (CT) or nearly so (J. L. Donley et al. 2010). Data from the Near-Infrared Spectrograph (NIRSpec; P. Ferruit et al. 2022; P. Jakobsen et al. 2022) show the classic "V-shape" feature at its core, similar to that seen in canonical LRDs. While its integrated SED differs somewhat from LRDs, its nuclear SED shows striking similarity, suggesting it may represent a more evolved descendant or an analog.

Notably, *the Saguaro* consists of a compact LRD-like nucleus *plus* a face on spiral galaxy surrounding it. This provides an opportunity to explore whether, at high redshift, it would appear as a compact LRD, or whether it would be disqualified by the surrounding structure. We explore this question both by synthetically moving it to z ≈ 7 and also by an analysis of the impact of surface brightness dimming on the detectability of LRD host galaxies in general.

This paper is organized as follows. In Section 2, we introduce *the Saguaro* and present its main observational characteristics. We then highlight its resemblance to canonical LRDs through three independent lines of evidence: (1) multiwavelength AGN–host image decomposition; (2) a spatially resolved NIRSpec/PRISM spectrum in its nuclear regions; and (3) a redshifting experiment illustrating how the system would appear if observed at higher redshifts. In Section 3, building on the findings from Section 2, we investigate, through stacking analysis, whether LRDs at $z \approx 4$–8 may similarly be embedded within faint extended emission that becomes increasingly suppressed with redshift due to cosmological surface brightness dimming. We then develop a simple analytic model quantifying the expected loss of detectable light from LRDs at increasing redshifts. In Section 4, we show that *the Saguaro* is not an isolated case. Finally, in Section 5, we discuss and summarize our findings.

Throughout this paper, we consider a cosmology with $H_0 = 70$ km s^{-1} Mpc^{-1}, $\Omega_M = 0.3$, and $\Omega_\Lambda = 0.7$. All magnitudes are total and refer to the AB system (J. B. Oke & J. E. Gunn 1983). A P. Kroupa (2001) initial mass function (IMF) is assumed (0.1–100 $M_\odot$).

2. *THE SAGUARO*: A CASE STUDY

The characteristic features of high-redshift LRDs are their "V-shaped" SEDs, typically emerging around 3600 Å in the rest frame (e.g., D. J. Setton et al. 2024), and their compactness in the Long Wavelength channel from NIRCam. They often have broad Balmer lines indicative of active black hole accretion. While this distinctive spectral shape has been predominantly observed at $z \gtrsim 3 - 4$, recent efforts have uncovered a few rare cases at lower redshifts (e.g., B. Wang et al. 2024; I. Juodžbalis et al. 2024). We propose another intriguing example at $z \approx 2$: *the Saguaro*, located in the GOODS-N field (R.A. = 189.1482812, Dec = 62.2400236), with an extensive multi-wavelength coverage ranging from X-ray to submillimeter wavelengths.

In this section, we present *the Saguaro* and describe its general properties. We show that it has a "V-shaped" SED, which arises from the bright central core of the galaxy, based on a multi-wavelength AGN–host image decomposition and a spatially resolved analysis of the NIRSpec/PRISM spectrum in its nuclear region. Finally, we investigate how this object would appear if observed at high redshifts, revealing a striking resemblance to canonical LRDs.

[21] In reference to the rare spiral-shaped crested Saguaros found in the Arizona desert; both are strikingly sculptural, with some of them being clearly spiral in form, and span impressive scales in their respective environments.

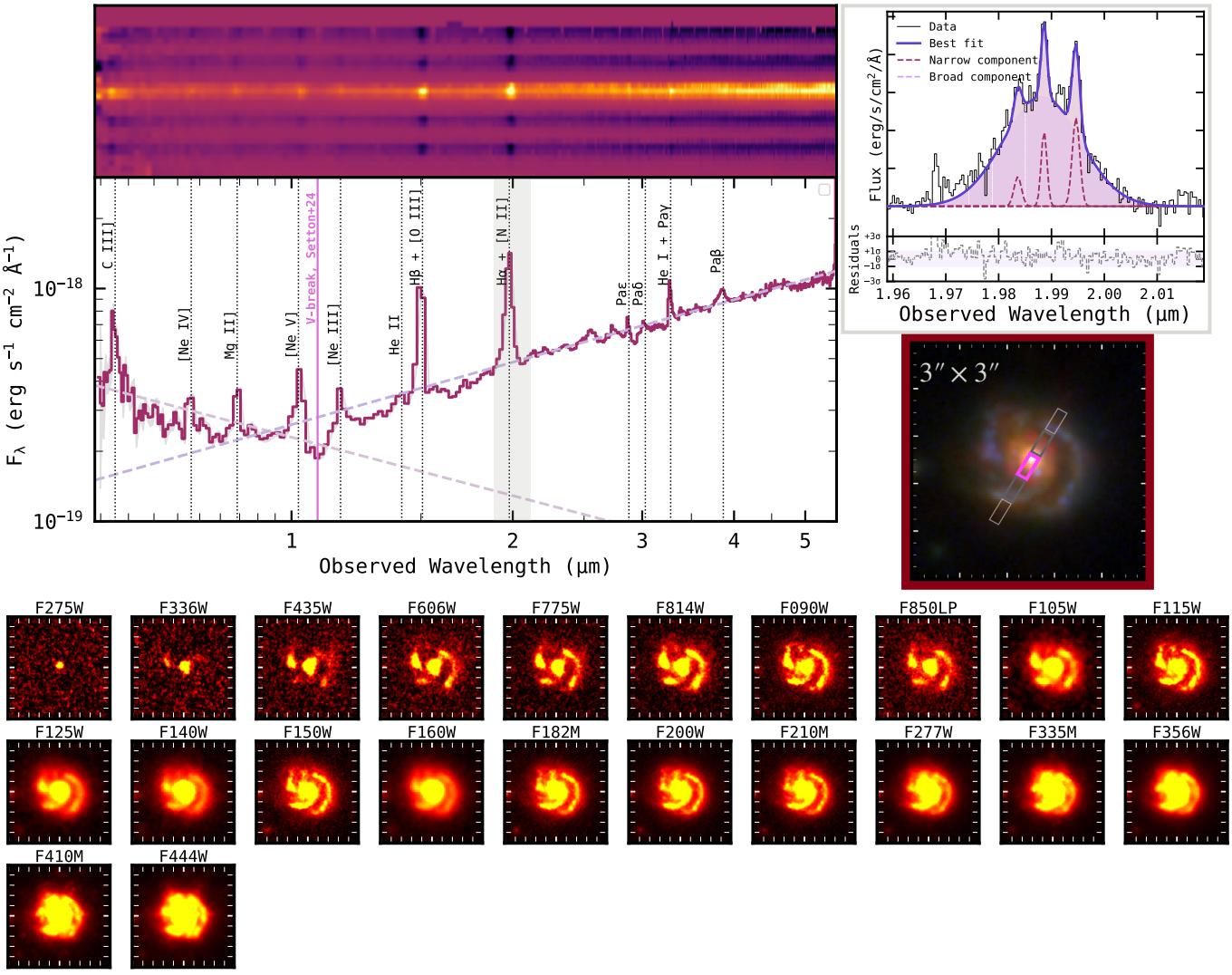

Figure 1. Top: On the left, we show the NIRSpec/PRISM spectrum of *the Saguaro* (from the DJA DAWN Archive), with all prominent emission lines labeled. The expected position of the "V-break", as defined by D. J. Setton et al. (2024), is marked in orchid. The Hα + [N II]$\lambda\lambda$6548, 6583 complex (unresolved in the PRISM spectrum) is highlighted in gray. Its higher-resolution counterpart from the NIRSpec G235H/F170LP grating is shown in the top-right panel, along with the line model fits for both Hα and [N II]$\lambda\lambda$6548, 6583. Finally, we show the NIRCam RGB image (3″×3″) of *the Saguaro* with the slit overlaid, illustrating that the PRISM flux originates from the nuclear regions. **Bottom:** Postage stamps (3″×3″) of the available HST and JWST filters for *the Saguaro*.

2.1. *Dataset*

We used both imaging and spectroscopic data from the GOODS-N field, obtained with the *Hubble* Space Telescope (HST) and JWST.

For HST, we relied on the *Hubble* Legacy Field (HLF) dataset, which provides broad wavelength coverage from 0.2 to 1.6 μm, including UV bands (WFC3/UVIS: F275W and F336W), optical bands (ACS/WFC: F435W, F606W, F775W, F814W, F850LP) and near-infrared bands (WFC3/IR: F105W, F125W, F140W, F160W). A detailed description is available in K. E. Whitaker et al. (2019)[22].

For JWST, we used both NIRCam and NIRSpec observations. NIRCam imaging was obtained from JADES/NIRCam Data Release 2 (DR2; PIDs: 1181; PIs: D. Eisenstein; D. J. Eisenstein et al. 2023a,b; F. D'Eugenio et al. 2024[23]), complemented by data from

[22] HLF imaging is publicly available at https://archive.stsci.edu/prepds/hlf/.

[23] JADES images available at https://archive.stsci.edu/hlsp/jades.

the FRESCO program (PID: 1895; PI: P. Oesch; P. A. Oesch et al. 2023). These images reach 5σ depths of 29.3–29.9 mag (measured in 0.15″-radius apertures; see F. D'Eugenio et al. 2024 for more details on the data reduction). NIRSpec observations were obtained as part of the NIRSpec GTO WIDE survey (PID: 1211, PI: K. Isaak; M. V. Maseda et al. 2024). We made use of both PRISM and G235H/F170LP data. The PRISM spectrum was initially obtained from the DAWN JWST Archive (see Figure 1, left). However, to properly assess whether the "V-shaped" SED was confined to the nuclear region, we re-reduced the data using MSAEXP[24] (`v0.9.8`; G. Brammer 2023) to avoid self-subtraction effects introduced by the default nodding technique (see Section 2.3.3 for details). The G235H/F170LP data were fully reduced with MSAEXP from the outset.

The Saguaro is also detected in the deep *Chandra* 2Ms X-ray data (Y. Q. Xue et al. 2016; `ID`: CDFN−190) with $L_{X,\,2-10\,\mathrm{keV},\,\mathrm{int}} = (6.61\text{–}10) \times 10^{43}\,\mathrm{erg\,s^{-1}}$ (J. L. Donley et al. 2010; A. Del Moro et al. 2016), with an absorbing column density of $N_H \approx 10^{23.6-23.8}\,\mathrm{cm^{-2}}$(D. M. Alexander et al. 2005; J. L. Donley et al. 2010). The source shows no detection in the Nuclear Spectroscopic Telescope Array (NuSTAR) data (F. A. Harrison et al. 2013). To validate the previous findings in the X-ray, we re-extracted and analysed all the *Chandra* observations using the Chandra Interactive Analysis of Observations (CIAO; v4.17 and CALDB 4.11.0; A. Fruscione et al. 2006) tools (`specextract`). The spectra from different observations (covering a span of 1.5 years) were combined in a single one via the CIAO tool `combine_spectra`. We did not find any significant variability in the covered time range. The object has an effective coverage of ≈ 1.96 Ms, with 246 net-counts (i.e. background subtracted). Given the number of counts, we performed the spectral analysis using unbinned data and C-statistic (W. Cash 1979). The limited counts above background and the high redshift of the source also constrained the spectrum to rest-frame energies $E > 3.5$ keV, meaning it is safe to assume the spectrum is not contaminated by host galaxy contributions.

2.2. *Properties of the Saguaro*

We leveraged the available data for *the Saguaro* to construct a comprehensive picture of the system: (1) Section 2.2.1 outlines the host galaxy properties; (2) Section 2.2.2 examines the morphology; (3) Section 2.2.3 details its X-ray properties; and (4) Section 2.2.4 derives its $M_\bullet$ and discusses its implications.

[24] https://github.com/gbrammer/msaexp

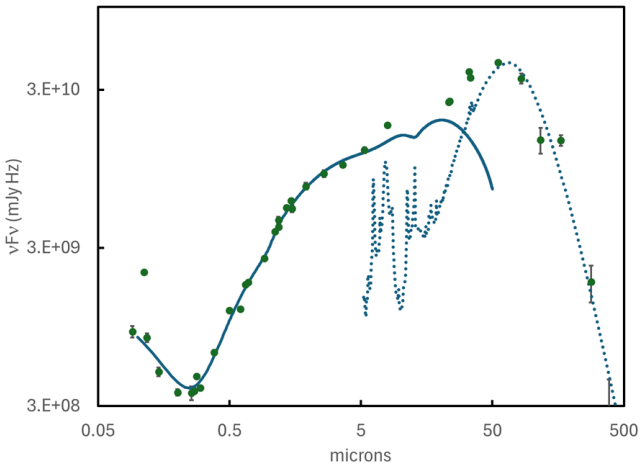

Figure 2. The SED of *the Saguaro*. The template of a $\log_{10}(L_{\mathrm{IR}}/L_\odot) = 11.5$ star forming LIRG (G. H. Rieke et al. 2009; dashed line) is shown fitted to the longest wavelengths and has been subtracted from the total to leave the SED of the nucleus (solid line) without the star-forming contribution.

2.2.1. *Host galaxy integrated properties*

Figure 1 provides an overview of *the Saguaro* and the HST and JWST data used to derive its properties. Stellar masses of $\log_{10}(M_\star/M_\odot) \approx 11.3$ have been derived using the FAST code from M. Kriek & C. Conroy (2013) in the recent literature (R. P. Naidu et al. 2017; D. Liu et al. 2018; N. J. Cleri et al. 2023), often based on photometry compiled by R. E. Skelton et al. (2014). However FAST depends strongly on rest-frame optical colors, which for this galaxy are heavily contaminated by the infrared excess (see Figure 2). Therefore, to ensure the robustness of the previous measurements, we redetermined the galaxy mass using the AGN-host decomposition (see Section 2.3.2) to obtain the intrinsic stellar SED, as illustrated in Figure 3, and running BAGPIPES (A. C. Carnall et al. 2019) for the synthesis modeling. We find $\log_{10}(M_\star) = 11.3 \pm 0.1$ (nominal uncertainties only). This confirms the previous values and appears to be inconsistent with the value of $\log_{10}(M_\star) \approx 10.46$ from A. Bongiorno et al. (2014)[25].

Previous works (e.g., J. L. Donley et al. 2010) suggest that *the Saguaro* hosts a deeply embedded AGN. To prove this, we selected the highest quality photometric measurements for this object from the recent literature to generate the SED shown in Figure 2 and listed in Table 1. We have decomposed the SED into two components: one according to a $\log_{10}(L_{\mathrm{IR}}/L_\odot) = 11.5$

[25] They already reported that the fit for this particular object was challenging (see their Section 4 and Figure 2).

Table 1. The SED measurements of *the Saguaro* compiled from the literature, corresponding to those shown in Figure 2.

rest-frame λ (μm)	νF_ν (mJy Hz)	Error (mJy Hz)	Reference
0.091	8.89E+08	7.42E+07	1
0.111	2.12E+09	3.61E+07	1
0.118	8.14E+08	5.37E+07	2
0.144	4.96E+08	3.23E+07	3
0.201	3.68E+08	1.70E+07	3
0.257	3.63E+08	3.63E+07	3
0.270	3.73E+08	1.49E+07	3
0.282	4.64E+08	8.50E+06	3
0.299	3.91E+08	3.33E+06	3
0.381	6.57E+08	2.09E+06	3
0.498	1.21E+09	2.60E+06	3
0.663	1.77E+09	2.38E+06	3
0.697	1.82E+09	2.14E+06	3
0.919	2.58E+09	2.17E+06	3
1.111	3.81E+09	1.90E+06	3
1.179	4.49E+09	2.25E+08	3
1.181	4.08E+09	1.58E+06	4
1.360	5.38E+09	2.20E+06	3
1.473	5.99E+09	1.86E+06	3
1.492	5.32E+09	2.66E+08	4
1.903	7.37E+09	3.69E+08	4
2.612	8.87E+09	4.43E+08	4
5.321	1.25E+10	5.61E+08	5
7.960	1.79E+10	5.24E+08	5
23.691	2.55E+10	3.40E+08	6
33.960	3.57E+10	9.23E+08	5
54.974	4.45E+10	1.48E+09	5
82.919	3.54E+10	2.63E+09	5
116.106	1.45E+10	2.69E+09	5
165.837	1.43E+10	1.09E+09	5
281.877	1.83E+09	4.80E+08	5
385.669	2.73E+08	1.68E+08	5

References: (1) P. A. Oesch et al. (2018); (2) C. Borys et al. (2005); (3) M. J. Rieke et al. (2023), JADES DR3 NIRCam photometry (GOODS-N v1.0; Extension 6) `circ0`, corrected to total flux (factor of 1.25); (4) H. I. Teplitz et al. (2011), All the IRAC measurements were reduced by a factor of 1.22 to bring them into agreement with the JADES photometry at similar wavelengths; (5) D. Liu et al. (2018); (6) D. J. Hanish et al. (2015)

LIRG template from G. H. Rieke et al. (2009) and the second as the remaining flux. The decomposition is non-degenerate for this case because of the extreme luminosity of the star-forming component, and the selected template is in agreement with the luminosity range found to fit the far infrared of galaxies in this redshift range (W. Rujopakarn et al. 2013).

The shape of the remaining SED (see Figure 2) indicates the presence of a very deeply embedded AGN. We will find that its luminosity approximates the Eddington limit for the embedded SMBH (Section 2.2.4), indicating that little luminosity escapes. J. L. Donley et al. (2010) show that the mid infrared spectrum is a virtually featureless power law rising rapidly toward longer wavelengths. Although some Hα escapes, the hydrogen lines are heavily obscured, as shown by Hβ not being detected. The source may be analogous to extreme objects like IRAS05189-2524 and IRAS08572+3915 (e.g., P. Severgnini et al. 2001; A. Efstathiou et al. 2014), deeply embedded AGNs with luminosities approaching 10^{12} L$_\odot$ but still letting sufficient light through to show AGN emission lines.

We can determine a star formation rate (SFR) from Figure 2. The total infrared luminosity from the star-forming template is 3.2×10^{12} L$_\odot$, corresponding to an integrated SFR of 500 M$_\odot$/yr, consistent with the result from A. Bongiorno et al. (2014) but somewhat lower than some of the previous estimates (e.g., A. Del Moro et al. 2016; N. J. Cleri et al. 2023). The specific SFR (sSFR) is then $\approx 10^{-8.60}\,\mathrm{yr}^{-1}$, which is exceptionally high for its redshift, placing it along the upper envelope of the Main Sequence of star-forming galaxies (J. S. Speagle et al. 2014; P. Popesso et al. 2023). The luminosity of the AGN component is then 4.6×10^{12} L$_\odot$, assuming essentially all of it emerges in the infrared.

2.2.2. *System morphology*

Figure 1 shows images of *the Saguaro* across the HST and NIRCam wavelength range. In the rest-frame UV, the emission is dominated by a compact central source surrounded by a faint halo, consistent with a face-on spiral host. As we move into the rest-frame optical, the extended galaxy becomes increasingly prominent (J. L. Donley et al. 2010). At redder wavelengths, the central core increasingly dominates the emission, as expected from the SED in Figure 2. This effect is visible across the individual bands (see Figure 1) and also in our AGN–host decomposition discussed later.

2.2.3. *X-ray properties*

To fit the X-ray spectrum, we chose a simple phenomenological model and a slightly more complex theoretical model. The phenomenological model is composed of a power-law, a neutral absorber at the redshift of the source, and a local neutral absorber to correct for the Galactic absorption. Due to the redshift of the source and the limited amount of counts, our

spectrum is limited to $E > 3.5\,\mathrm{keV}$, making it challenging to fit at the same time both the power-law slope and the source obscuration; therefore, we fixed the photon index to a canonical $\Gamma = 1.8$. The spectrum is well fitted by our simple model, and neither additional soft emission or reflection components improve our fit significantly. Our fit provides an obscuration of $N_H = (3.4^{+1.0}_{-0.8}) \times 10^{23}\,\mathrm{cm}^{-2}$ and an intrinsic (i.e. absorption-corrected) 2-10 keV (rest-frame) luminosity of $L_{2\text{–}10\,\mathrm{keV}} = (7.9^{+2.1}_{-1.6}) \times 10^{43}\,\mathrm{erg\,s}^{-1}$.

We tried to physically model the spectrum via the MYTorus model (K. D. Murphy & T. Yaqoob 2009), which self-consistently accounts for photoelectric absorption, Compton scattering, and fluorescent line emission in a toroidal geometry. MYTorus assumes a uniformly dense, toroidal obscurer with a fixed half-opening angle of 60°. This model can be used in both "coupled" and "decoupled" modes (T. Yaqoob 2012), the latter of which mimics a patchy/clumpy absorber, making it well-suited for studying moderately to heavily obscured sources. We utilized MYTorus in its "coupled" configuration and due to the low number of counts, certain parameters were fixed during fitting. Namely the slope at $\Gamma = 1.8$, and the scaling factors of the scattered continuum and line emission were both fixed at 1. We found results consistent with those from the phenomenological modeling, and obtained a torus obscuration along the line-of-sight of $N_{H,\mathrm{los}} \gtrsim 2.6 \times 10^{23}\,\mathrm{cm}^{-2}$, an inclination angle of $\geq 60°$, and an intrinsic luminosity of $L_{2\text{–}10\,\mathrm{keV}} = (7.5^{+1.3}_{-1.1}) \times 10^{43}\,\mathrm{erg\,s}^{-1}$. All in all, our measurements are consistent with the previous literature.

From our estimate of the intrinsic X-ray luminosity and using the infrared luminosity of the AGN component as L_{bol}, we estimate the bolometric correction factor ($k_{\mathrm{bol}} \equiv L_{\mathrm{bol}}/L_{\mathrm{X,\ 2\text{–}10\ keV,\ int}}$) to be ≈ 200. For an AGN of the appropriate luminosity, the expected value is ≈ 50 (F. Duras et al. 2020; C. Auge et al. 2023). This suggests that the intrinsic X-ray luminosity has been underestimated by as much as a factor of four, or that the source is modestly X-ray weak.

As a check on this result, we have derived L_{bol} from [Ne v]λ3426, which can be used as a tracer of L_{bol} in obscured AGNs (e.g., R. Gilli et al. 2010; L. Barchiesi et al. 2024). We adopted the calibration presented in L. M. Feuillet et al. (2024)[26] (see their Section 4), where $(L_{\mathrm{bol}}/\mathrm{erg\,s}^{-1}) = 0.94\ \log_{10}(L_{[\mathrm{Ne\,v}]\lambda3426}/\mathrm{erg\,s}^{-1}) + 6.51$. We model the [Ne v]$\lambda$3426 line from NIRSpec/PRISM data with both MSAEXP and our internal pipeline, obtaining a consistent flux of $(9.03 \pm 0.71) \times 10^{-17}\,\mathrm{erg\,s}^{-1}\,\mathrm{cm}^{-2}$, corresponding to $L_{\mathrm{bol}} \approx (2.56 \pm 0.22) \times 10^{46}\,\mathrm{erg\,s}^{-1}$, where the uncertainty is driven primarily by the signal-to-noise of the line. The correlation itself is established at $\approx 4.5\sigma$ (L. Barchiesi et al. 2024), so the final estimate is $(6 \pm 1.5) \times 10^{12}\ \mathrm{L}_{\odot}$, consistent with our result from integrating the infrared SED associated with the AGN[27]. This lends additional support to attributing this source component to an embedded AGN.

To further assess the true X-ray nature of this source, we examine the relation between the rest-frame UV and X-ray monochromatic luminosities, specifically $L_{2500\,\text{Å}}$ and $L_{2\,\mathrm{keV}}$, via the optical-to-X-ray index (α_{OX}). Without applying any dust correction to $L_{2500,\text{Å}}$, we derive $\alpha_{\mathrm{OX}} \approx -1.25$, which is consistent with typical AGN values (e.g., E. Lusso & G. Risaliti 2016). We note that this relation was calibrated primarily for unobscured AGNs. However, the source exhibits a high k_{bol} (≈ 200), suggesting a potential discrepancy. This apparent inconsistency may arise from residual X-ray absorption not fully accounted for by the applied column density, or alternatively, may reflect an intrinsically X-ray-weak central engine. Reconciling the observed α_{OX} with a value indicative of X-ray weakness (e.g., $\alpha_{\mathrm{OX}} \approx -1.8$) would require a dust extinction of $A_V \approx 2$ mag, assuming a Calzetti reddening law (D. Calzetti et al. 2000). While this is slightly higher than the upper limit of A_V inferred from our BAGPIPES SED modeling, the values remain broadly consistent within the uncertainties and potential systematics in the SED modeling. The detection of broad Hα emission but no Hβ further supports a partially obscured geometry in which both the narrow-line region and portions of the broad-line region are visible. However, the observed X-ray faintness is likely the result of a combination of factors: the source is highly obscured, severely attenuating the intrinsic emission, and intrinsically X-ray weak, possibly due to a suppressed or underluminous corona. We note that a similar case was recently presented in another SMG at a higher redshift by E. Parlanti et al. (2024).

2.2.4. *Properties of the SMBH*

The Saguaro is covered by NIRSpec G235H/F170LP observations, which we reduced using MSAEXP. Its spectrum reveals a broad Hα component (see Figure 1) with $F(\mathrm{H}\alpha) = (1.03 \pm 0.05) \times 10^{-16}\ \mathrm{erg\,s}^{-1}\,\mathrm{cm}^{-2}$

[26] Adapted from the calibration proposed in S. Satyapal et al. (2007) and rescaled to [Ne v]λ3426 as discussed in L. M. Feuillet et al. (2024).

[27] In contrast, N. J. Cleri et al. (2023) measured the [Ne v]λ3426 line from HST/WFC3 G102 slitless grism spectroscopy and obtained a flux almost twice as large as ours. This would imply a significantly higher bolometric luminosity obtained from the infrared SED and we do not make use of it.

and a FWHM of 2521 ± 256 km s^{-1}. We also detect the [N II]$\lambda\lambda$6548, 6583 doublet with a flux ratio of 3.01 ± 0.52, in agreement, within uncertainties, with the theoretical value of 3.05 (I. Dojčinović et al. 2023). The broad Hα was also found in previous works by A. M. Swinbank et al. 2004, A. Bongiorno et al. (2014), and G. D. Wirth et al. 2015.

Because of the complexities in interpreting the Hα flux (and no information about Hβ with the high resolution grating) and the local intrinsic AGN continuum, we have used the X-rays to estimate the black hole mass. We follow the calibration from S. LaMassa et al. (2025). However, we need to correct for the very large $k_{\rm bol}$ (200) compared with the relation assumed there (E. Lusso et al. 2010). The result is $\log_{10}(M_\bullet/M_\odot) = 8.12$, with errors that are difficult to estimate because of the complexities in determining the intrinsic X-ray properties. This is consistent with the prior estimate of $\log_{10}(M_\bullet/M_\odot) = 7.99 \pm 0.3$ by A. Bongiorno et al. (2014), but is higher because of our allowance for the large $k_{\rm bol}$. Thus, the resulting Eddington Limit is 4.2×10^{12} $L_\odot$, essentially the same as our value for the AGN luminosity, i.e., the source is accreting close to the Eddington rate. The nucleus is broadly along the local $M_\bullet$–$M_\star$ relation (J. E. Greene et al. 2016) with $M_\bullet/M_\star \approx 0.0004$, i.e. within the scatter in that relation and the uncertainties in $M_\bullet$ and $M_\star$.

2.3. *Resemblance to LRDs*

In this section, we emphasize the similarity between *the Saguaro* and canonical LRDs by focusing on two defining features: its characteristic "V-shaped" SED (Section 2.3.1), which we show originates from the central region (Sections 2.3.2–2.3.3), and the unresolved, point-like morphology it would present if observed at high redshift (Section 2.3.6). Moreover, we show that its sub-mm and X-ray detections do not contradict its resemblance to LRDs (Sections 2.3.4–2.3.5).

2.3.1. *The V-shape of the Saguaro*

The NIRSpec/PRISM spectrum of *the Saguaro* provides one of the clearest examples of a "V-shaped" spectrum, emerging at a rest-frame wavelength comparable to those observed in canonical LRDs. We measure UV and optical slopes of -0.812 and 0.901 (see Figure 1), respectively. We find the spectrum is fully consistent with the definition of canonical LRDs proposed by D. D. Kocevski et al. (2024). We show these slopes in Figure 1. We also display the expected "V-break" at rest-frame $\approx$ 3600 Å, as reported by D. J. Setton et al. (2024). Interestingly, the "V-shaped" spectrum is observed in NIRSpec/PRISM data that sample nearly the central region of the galaxy, with the shutter positioned close to its nucleus.

2.3.2. *Multiwavelength AGN-host image decomposition*

We further validate the "V-shaped" spectrum of *the Saguaro* using multiband photometric decomposition to separate the AGN from its host galaxy. We employ the `GALFITM` package (B. Häußler et al. 2013), an extension of the widely used `GALFIT` software (C. Y. Peng et al. 2002, 2010), to simultaneously model our NIRCam and HST images, allowing parameter variations as functions of wavelength. This method effectively leverages multiband data, producing more robust fits compared to single-band decompositions, while accounting for morphological wavelength variations. `GALFITM` has been widely utilized for structural decompositions of AGN-host galaxy systems at cosmic noon (e.g., M.-Y. Zhuang & L. C. Ho 2023; M. Zhuang et al. 2023; S. Gillman et al. 2025).

We model the AGN as a point source and the host galaxy with a single Sérsic profile to capture its dominant structure. While the host exhibits spiral arms, they are far enough from the galactic center that they do not contaminate the AGN flux significantly. Our Sérsic model thus represents the azimuthally averaged light profile of the disk. A more complex decomposition, incorporating a galactic bar and a nearby stellar clump, located 0.18″ southwest of the nucleus, is presented later in this section. However, we adopt the simpler AGN–galaxy decomposition as our fiducial result, since it captures the dominant components while avoiding parameter degeneracy associated with more complex models. We do not include a bulge component, as neither the NIRCam nor HST images reveal a prominent bulge component. If present, the bulge is likely a pseudo-bulge: classical bulges typically have effective radii larger than 1 kpc (P. Dimauro et al. 2019), which would be resolved by NIRCam. For example, the FWHM of the NIRCam/F200W PSF is 0.064″, corresponding to 0.55 kpc at $z = 2$, smaller than the typical radius of a classical bulge. Pseudo-bulges generally have bulge-to-total flux ratios below 0.2 (D. B. Fisher & N. Drory 2008), and since *the Saguaro* is brighter than its host in most bands, any contribution from a pseudo-bulge is likely minor.

In the `GALFITM` configuration, we use Chebyshev polynomials to model the wavelength dependence of structural parameters, allowing for smooth variation across filters while mitigating overfitting. The magnitudes of both the AGN and Sérsic components are left free in all bands. The Sérsic index and half-light radius are allowed to vary quadratically with wavelength, following

the approach of B. Häußler et al. (2013) and M. Zhuang et al. (2023), which provides sufficient flexibility to capture real structural changes while maintaining stability in low signal-to-noise filters. To avoid introducing artificial wavelength-dependent distortions, we fix the ellipticity and position angle across all bands. We also assume the AGN and host galaxy share a common center, fixed in all bands. Nearby galaxies are manually masked in the decomposition.

We present our results in Figure 3, which shows the modeled photometry for both the host galaxy and the AGN, each normalized to match the NIRSpec/PRISM spectrum, along with the spectrum itself. The AGN–host decomposition reveals that the characteristic "V-shaped" SED is well reproduced by the point-like source used to model the AGN component, distinct from the SED of the host galaxy. If one were to consider only the integrated photometry of this system and apply standard selection criteria for LRDs, such as color cuts and compactness thresholds (e.g., G. Barro et al. 2024a,b; J. E. Greene et al. 2024; V. Kokorev et al. 2024; P. Rinaldi et al. 2024) or even the criterion from D. D. Kocevski et al. (2024), this object would likely be missed. However, when the two components are separated, the AGN component alone would satisfy the LRD selection criteria. This raises the question of whether such criteria need to be fine tuned when looking for lower-z counterparts of LRDs. It also underscores the importance of disentangling central emission from that of the extended host when attempting to identify potential analogs at lower redshifts. A similar conclusions has been also suggested recently by J.-B. Billand et al. (2025).

The host galaxy properties are consistent with normal disk galaxies. The half-light radius of the host galaxy is 5.8 kpc at rest-frame 0.15 μm and decreases to 3.7 kpc at 1.5 μm, consistent with the known trend of decreasing size with wavelength (e.g., B. Vulcani et al. 2014). The measured Sérsic index remains near $n \approx 1$ across all bands, typical of disk galaxies. The SED of the host galaxy, as shown in Figure 3, resembles that of normal spiral galaxies in the local universe (M. J. I. Brown et al. 2014), showing a Balmer break and a downturn beyond ≈ 2 μm (rest-frame 0.7 μm), in contrast to the steeply rising AGN SED. In the rest-frame UV, the F_λ decreases with wavelength, but the slope is flatter than that of the AGN.

Interestingly, residuals near the galaxy center reveal asymmetric, off-center features located $\approx 0.1''(\approx 0.8\,\mathrm{kpc})$ from the nucleus. This structure is unlikely to be a bulge given its offset from the nucleus. It resembles the off-center blobs seen in LRDs by C.-H. Chen et al. (2025a), which they suggest might be merging companion galaxies, disturbed host structures, or AGN-illuminated nebular emission. Notably, *the Saguaro* has two neighboring galaxies to the east and southeast at projected distances of 24 and 26 kpc. Their JADES photometric redshifts from the JADE catalog are 2.04 and 2.03, respectively, consistent with the spectroscopic redshift of *the Saguaro* ($z = 2.0145$), suggesting potential physical association. If spectroscopically confirmed, they could possibly be evidence of ongoing minor mergers. Alternatively, the asymmetric, off-center features could be also a stellar clump near the nucleus, which is common seen in $z \approx 2$ galaxies (e.g., B. S. Kalita et al. 2024).

Finally, we tested a sophisticated model including a bar and a stellar clump in the modeling, fitted alongside the AGN and disk. The clump, located $0.18''$ southwest of the nucleus, is clearly seen in short-wavelength images. The bar, oriented northeast–southwest, is most prominent at long wavelengths, likely due to relatively older stellar populations common in bars. The bar is modeled with a Sérsic profile with a center tied to the disk. The fluxes across multiple bands are allowed free, while the Sérsic and radius are allowed to vary quadratically with wavelengths. The stellar clump is modeled as a point source. We find an improvement of residuals, and the AGN SED retains its V-shape. However, the added complexity introduces degeneracies and unphysical wiggles. For example, in the F200W band, where the bar is not visible, the model increases bar flux to account for the asymmetric, extended feature mentioned above, and thus reduces the inferred AGN flux. Moreover, at long-wavelengths, the stellar clump is blended with the AGN due to lower resolution. To avoid such artifacts, we adopt the simpler AGN–Sérsic decomposition as our baseline. The sophisticated model confirms that contamination from the substructures is $< 10\%$, so it does not affect our main conclusions.

Although the AGN–host decomposition reveals the spatial coincidence of the AGN with the observed "V-shaped" SED feature, it remains unclear whether it arises solely from AGN activity or is also influenced by an additional component, such as hot, young stars in a circumnuclear starburst ring. These structures are commonly observed in the central regions of active galaxies at low redshift ($z \lesssim 0.1$). Although they have typical radii $\gtrsim 0.5$ kpc (e.g., J. K. Kotilainen et al. 2000; T. Bohn et al. 2023), which would be resolved with NIRCam at the redshifts probed here ($z \approx 2$), it remains uncertain whether similar structures exist on smaller, unresolved spatial scales. In this regard, ALMA observations have revealed a more complex picture in the nu-

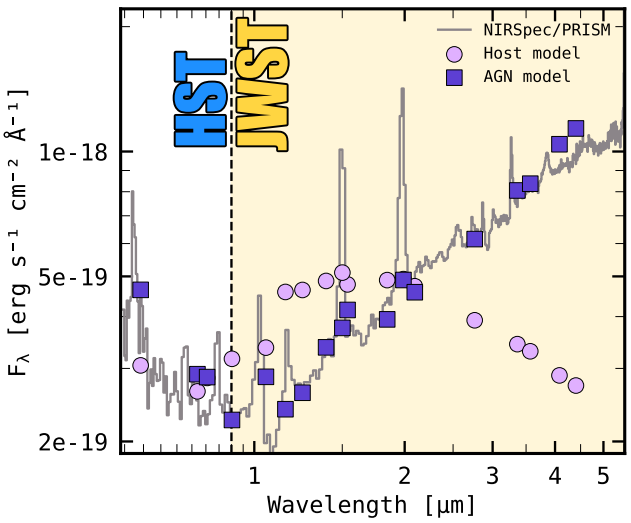

Figure 3. The NIRSpec/PRISM spectrum of *the Saguaro* (using the standard reduction from the DAWN JWST Archive), shown alongside the AGN–host decomposition photometry from GALFITM, scaled to match the NIRSpec/PRISM flux level. The vertical line indicates the transition from HST to JWST coverage, below which the UV photometry is provided solely by HST.

clear regions of high-z galaxies, often showing clumpy, compact star formation and gas distributions (e.g., R. Gilli et al. 2014; J. A. Hodge et al. 2019), which may cause contamination to our AGN SED.

2.3.3. *The "V-shape" lives at the center of the galaxy: insights from NIRSpec/PRISM*

The multiwavelength AGN–host image decomposition revealed that the "V-shaped" SED arises primarily from the AGN component used to model the central source. To investigate this detail, we further analyzed the NIRSpec/PRISM observations, which cover the central region of the object (see Figure 1). In particular, we performed an *ad hoc* reduction of the NIRSpec/PRISM data using MSAEXP. However, instead of the default nodding technique (adopted by the DAWN JWST Archive), which can suppress extended emission in the outskirts, we applied a customized background subtraction method following the procedure described in A. de Graaff et al. (2025b), now fully implemented in MSAEXP. In this approach, a global master sky spectrum is subtracted rather than using image differencing, effectively avoiding self-subtraction and preserving any extended structure. This strategy is essential to determine whether the "V-shaped" feature is truly concentrated in the nuclear region of *the Saguaro*, as it maximizes the recovered flux across the entire spatial profile.

By preserving the full spatial structure in the 2D spectrum and avoiding the background suppression due to default nodding techniques, we were able to extract one-dimensional spectra at each spatial pixel along the cross-dispersion axis, including those just beyond the nuclear regions of the galaxy. As described in the previous section, the AGN–host decomposition performed with GALFITM provided photometry for both the compact central AGN and the more extended host component. Therefore, for each spatial row, we compare the extracted spectrum with the corresponding AGN–host decomposed photometry, normalized to the flux level of the extracted spectrum.

We show the extracted spectra in Figure 4. While this analysis pushes the NIRSpec/PRISM data to its limits, it clearly reveals a strong contrast between the central "V-shaped" SED and the surrounding regions. The characteristic "V-shape" is most prominent within the central $\approx$ 0.1–0.2″(corresponding to $\approx$ 0.8–1.5 kpc at $z = 2.0145$). Although the spatial resolution of the NIRSpec/PRISM spectrum is limited to 0.1″/px, thus significantly lower than that achievable with NIRCam imaging, we still observe a clear transition in spectral shape beyond $\approx$ 0.1–0.2″ from the center, where the "V-shape" becomes less pronounced and gives way to a different continuum in the surrounding regions. This spatial variation is consistent with the AGN–host decomposition derived from GALFITM, reinforcing that "V-shaped" SED arises mostly from the innermost regions of the galaxy.

These findings also underscore the importance of slit placement in detecting such features. The presence and detectability of a "V-shaped" SED *could* strongly depend on whether the aperture or shutter covers the nucleus. This suggests that similar features may be missed in other galaxies due to slight misalignments, potentially hiding such cores within seemingly normal systems.

2.3.4. *The submillimeter flux*

The current strong submm flux seen in *the Saguaro* is clearly in violation of the properties of canonical LRDs (C. M. Casey et al. 2025). However, as shown in Figure 2, this is completely driven by the very high rate of star formation, which is likely to deplete the interstellar gas and fade quickly ($\lesssim$ 20 Myr) (e.g., N. M. Förster Schreiber et al. 2003) with an upper limit of 20–60 Myr set by the gas depletion timescale (F.-Y. Liu et al. 2024). This could leave a dust enshrouded AGN that emits weakly in the submm (unless it has successfully blown away its cocoon). In any case, ULIRGs and high Eddington ratio AGNs are not strongly correlated (G. H. Rieke et al. 2025), so this source component does not seriously undermine the analogy with LRDs.

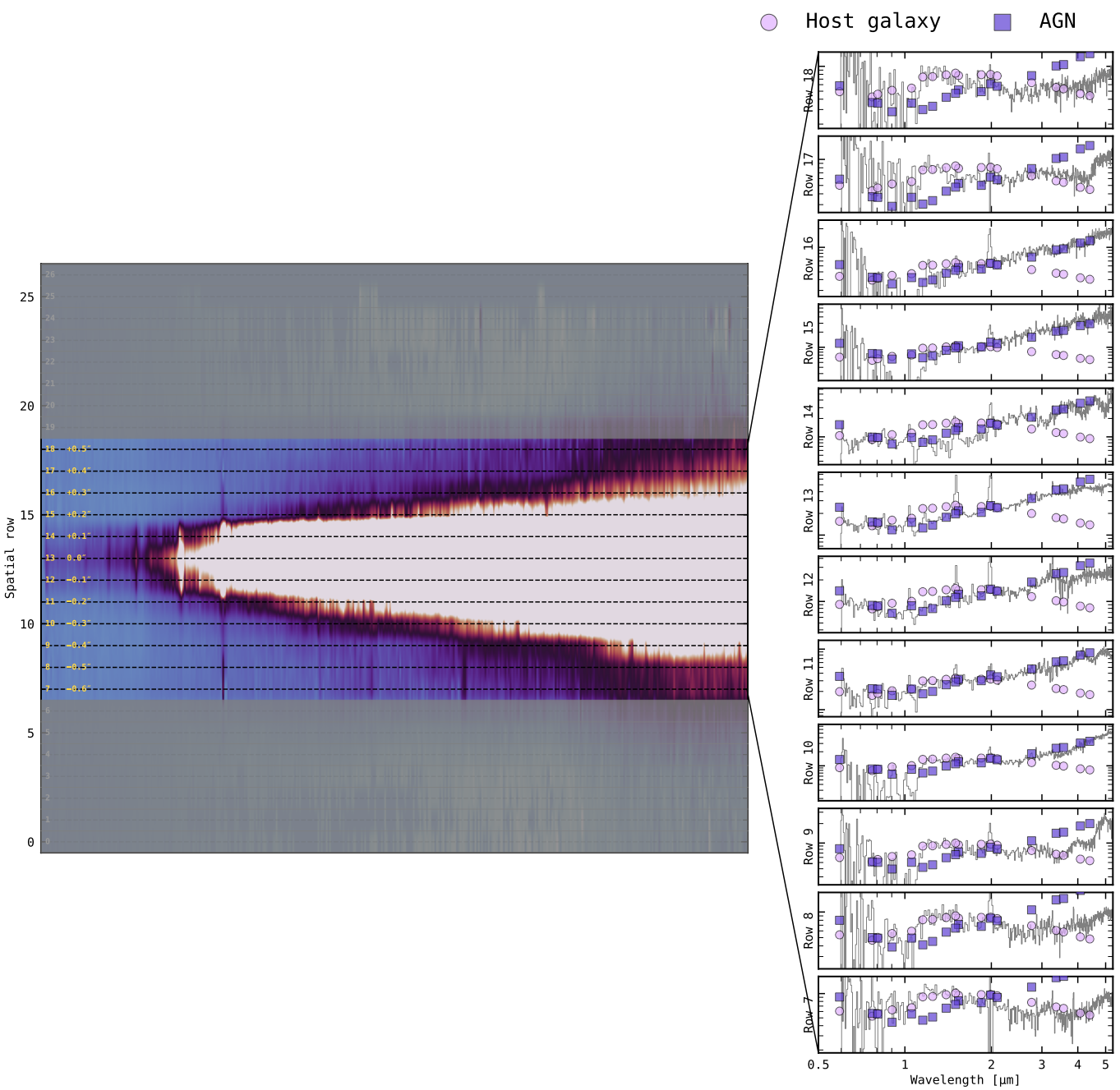

Figure 4. Extraction of row-by-row 1D spectra from the NIRSpec/PRISM 2D data of *the Saguaro*. Spectra are shown in F_λ vs. λ. Each subplot on the right shows the extracted spectrum (gray) for a given spatial row, along with the corresponding host galaxy and AGN photometry (from GALFITM) normalized to match the extracted spectrum at each row. The center of the trace is located at row 13. We also report the distance from the center of the spectral trace.

2.3.5. *The X-ray detection*

Recent studies have shown that LRDs are notoriously difficult to detect in the X-ray regime, with only two confirmed cases to date: PRIMER-COS 3866 at $z = 4.66$ and JADES 21925 at $z = 3.1$ reported in D. D. Kocevski et al. (2024). In most cases, stacking analyses of X-ray data (e.g., T. T. Ananna et al. 2024; M. Yue et al. 2024) have failed to yield significant detections, leading to the conclusion that these sources are intrinsically X-ray faint. At first glance, *the Saguaro* might appear to be an exception. However, our X-ray analysis indicates that this source is likely both X-ray weak *and* very obscured, based on its bolometric correction ($k_{\rm bol} \approx 200$) and its low $\alpha_{\rm OX}$ (when corrected for dust). Notably, when we compare our inferred X-ray luminosity with

upper limits from stacking analyses (e.g., T. T. Ananna et al. 2024; M. Yue et al. 2024), we find consistent results. We therefore conclude that the X-ray detection of *the Saguaro* does not contradict its resemblance to the LRD population.

2.3.6. *How we wonder what you would have looked like in the early Universe*

We showed that *the Saguaro* exhibits a "V-shaped" spectrum originating from its nuclear region, with the "V-break" occurring at the characteristic wavelength reported in the literature (D. J. Setton et al. 2024). We then demonstrated that AGN–host image decomposition confirms the spatial coincidence of this spectral shape with the central AGN. Finally, we highlighted that its sub-mm flux and X-ray detection do not violate its resemblance to the broader LRD population. This strong resemblance to LRDs naturally raises the question of whether this object could be considered a low-redshift analog. However, some key differences must be taken into account. First, compactness is a defining characteristic of LRDs, whereas our object (considering both AGN and host) is clearly extended. Second, *the Saguaro* is observed at $z \approx 2$, while canonical LRDs are typically observed at $z \gtrsim 4$–5. Additionally, its face-on disk morphology and far-infrared properties differ significantly from what is currently known about LRDs (although the latter may be a transient phase). These differences could reflect evolutionary changes over cosmic time.

This ambiguity makes a compelling case for investigating whether it can be considered as a possible analog of canonical LRDs at later epochs. Therefore, we investigate how *the Saguaro* would appear if observed (unchanged in its intrinsic properties) at higher redshifts. We emphasize that this is a simplified, toy experiment.

Nevertheless, this exercise raises important questions about whether current observations of LRDs at high redshift are systematically biased in recovering host galaxy properties, as recently suggested by F. Pacucci & A. Loeb (2025) and J.-B. Billand et al. (2025). In this regard, P. Rinaldi et al. (2024) has already shown that approximately 30% of photometrically selected high-redshift LRDs exhibit complex or disturbed morphologies, underscoring the need to carefully consider observational limitations, such as image depth, which might bias this fraction.

To investigate how cosmological surface brightness dimming (R. C. Tolman 1930) affects the detectability of extended emission in *the Saguaro* at high redshifts, we performed pixel-by-pixel SED fitting using EazyPy (G. B. Brammer et al. 2008). We adopted the `BLUE_SFHZ_13` template set along with an AGN+torus template, which includes redshift-dependent star formation histories and dust attenuation. The fit was restricted to NIRCam bands only, taking advantage of their superior spatial resolution. All bands were PSF-matched to F444W using STPSF (M. D. Perrin et al. 2014), and SEDs were extracted from each pixel after masking nearby contaminants. The redshift was fixed to that of the galaxy derived from the NIRSpec/PRISM spectrum.

Each pixel's SED was then redshifted to the target redshift, and the galaxy's appearance at earlier cosmic times was reconstructed following a FERENGI-like methodology (M. Barden et al. 2008). This includes angular size rescaling using the proper angular diameter distance ratio, full $(1+z)^{-4}$ surface-brightness dimming, and bandpass shifting. An evolutionary brightening term was also applied (see next paragraph). The redshifted SEDs were projected onto a blank canvas, convolved with the corresponding PSF, and injected into a real background extracted from a region close to the source. The background was cleaned by masking sources and replacing contaminated regions with nearby noise samples to preserve realistic structure and depth.

We stress that for this toy experiment, our goal is purely to visualize how cosmological surface-brightness dimming affects the extended host galaxy. To that end, we adopt the phenomenological prescription implemented in FERENGI, applying a uniform brightening of $M_{\rm evo}(z) = x\,z + M_0$ with $x = -1$ (M. Barden et al. 2008). Following the discussion in M. Barden et al. 2008, this choice is made purely for visual purposes, to illustrate the impact of surface-brightness dimming with redshift. We note that a physically realistic treatment would require evolving the AGN and host components separately, with the AGN scaled according to the evolution of the quasar bolometric luminosity function (e.g., X. Shen et al. 2020; H. Zhang et al. 2024), and the host following the stellar mass-to-light evolution observed in star-forming galaxies (e.g., T. Treu & L. V. E. Koopmans 2004).

We show the results of this toy experiment in Figure 5, which showcases three RGB images: the real object (on the left), its simulated appearance at $z = 7$ (at the center), and, for comparison, a representative LRD at similar redshift (on the right). This experiment demonstrates how cosmological surface-brightness dimming preferentially suppresses low-surface-brightness emission in galaxy outskirts while leaving compact central components detectable. This differential effect, which is consistent with the findings of V. Calvi et al. (2014), highlights how extended stellar light can easily fall below detection thresholds at high redshift, potentially ex-

plaining the lack of extended host galaxies around LRDs as redshift increases.

3. HOW MUCH WE NEVER SEE: ARE LRDS EMBEDDED IN EXTENDED HOSTS?

3.1. *The stacked UV profile of LRDs*

At the end of the previous section, we showed that *the Saguaro* (1) exhibits a "V-shaped" SED at its center, as revealed by both the AGN–host decomposition and the spatially resolved NIRSpec/PRISM spectrum, and (2) that if redshifted to high redshift (unchanged in its properties), the cosmological surface brightness dimming would preferentially suppress flux from the outskirts, leaving only the central AGN visible. Given the striking resemblance between *the Saguaro* and LRDs, and taking into account the intrinsic size evolution of galaxies with redshift (e.g., K. Ormerod et al. 2024; A. Genin et al. 2025), this naturally raises the question of whether observational biases significantly affect our current view of canonical LRDs at high redshift.

To explore this possibility, we analyzed the sample of 99 photometrically selected LRDs at $z \approx 4$–8 presented in P. Rinaldi et al. (2024), noting that not all of them necessarily host an AGN[28]. We stacked all sources using filters probing the rest-frame UV range of 1500–2000 Å (F090W, F115W, and F150W), after PSF-matching each image with STPSF to the reddest available filter in that wavelength range (F150W). Median-stacked cutouts were centered on the LRD positions, enhancing coherent low-surface-brightness features while suppressing outliers. To ensure that the stack captures only emission associated with the LRDs, all sources beyond $0.3''$ from the center were masked out prior to stacking. This method enables the isolation of extended UV emission.

We then derived the radial surface brightness profile of the stacked image and compared it to two PSF references: (1) the nominal PSF used for matching (F150W), and (2) a simulated stacked PSF created by repeating our full stacking procedure on synthetic NIRCam PSFs. To ensure realism, we applied random V3-angle rotations and spatial offsets before stacking, mimicking the astrometric and orientation variations present in the real dataset. We adopted a 1-pixel shift in both x and y, corresponding to 30 mas for the NIRCam short-wavelength channel. No significant dependence is found on the V3 angles, while the results are strongly sensitive to the applied offset. In our case, the applied offset (30 mas) is deliberately exaggerated (approximately six times the typical internal astrometric scatter in the JADES images) to highlight the reality of the extended host UV emission associated with LRDs.

Figure 6 (on the left) shows the result assuming a conservative background subtraction, where the outermost profile points are not allowed to average negative. Figure 6 (on the right) applies a more aggressive subtraction, allowing for negative values in the outskirts. In both cases, significant excess emission is seen beyond the PSF, extending to a radius of $\approx 0.2''$, or ≈ 2–3 kpc in diameter. The agreement between the two profiles down to a normalized intensity of 10^{-2} supports the robustness of this detection. This is also consistent with the recent findings of X. Lin et al. (2024), who analyzed a sample of broad Hα emitters at $z \approx 4-5$. However, their sources were not explicitly selected as LRDs and were drawn from a significantly smaller sample, yet the results are similar.

Interestingly, we repeated the same stacking analysis using only the subset of LRDs with spectroscopic redshifts (26 galaxies in total; JADES collaboration, in prep.). Although this subset represents a modest fraction (approximately 26%) of the full sample, the results remain unchanged, even when applying aggressive background subtraction. We also repeated the experiment excluding the galaxies classified as having "complex UV morphology" in P. Rinaldi et al. (2024), and found consistent results, further supporting the idea that canonical LRDs may reside within extended, low-surface-brightness envelopes.

Moreover, when examining the stacked images in successive redshift bins[29] ($z \approx 4$–5.8, $z \approx 5.8$–7, $z \approx 7$–8), we observe a slight evolution in the extent of the radial profiles from $z \approx 7$–8 to $z \approx 4$–5.8, consistent with the expected size evolution of galaxies across this range (e.g., K. Ormerod et al. 2024; A. Genin et al. 2025). We show this in Figure 7. Interestingly, we also find that objects below $z \approx 5$ fall almost entirely in the subsample of LRDs showing complex UV morphology. The number of such LRDs drops significantly from $z \approx 5$ to $z \approx 8$, with only two objects above $z > 7$ still showing clear morphological complexity. This naturally raises the question of whether this is a true effect, where as soon as the Universe matures, these objects start building more extended envelopes or whether this is a selection effect (J.-B. Billand et al. 2025). In the latter case, given the small sample size, we caution that the results

[28] However, diagnostic diagrams based on emission lines likely indicate a mixed origin, involving both star formation and AGN activity (P. Rinaldi et al. 2024).

[29] The bins were selected to ensure sufficient statistics in each, accounting for the redshift evolution in the number density of LRDs (D. D. Kocevski et al. 2024; V. Kokorev et al. 2024).

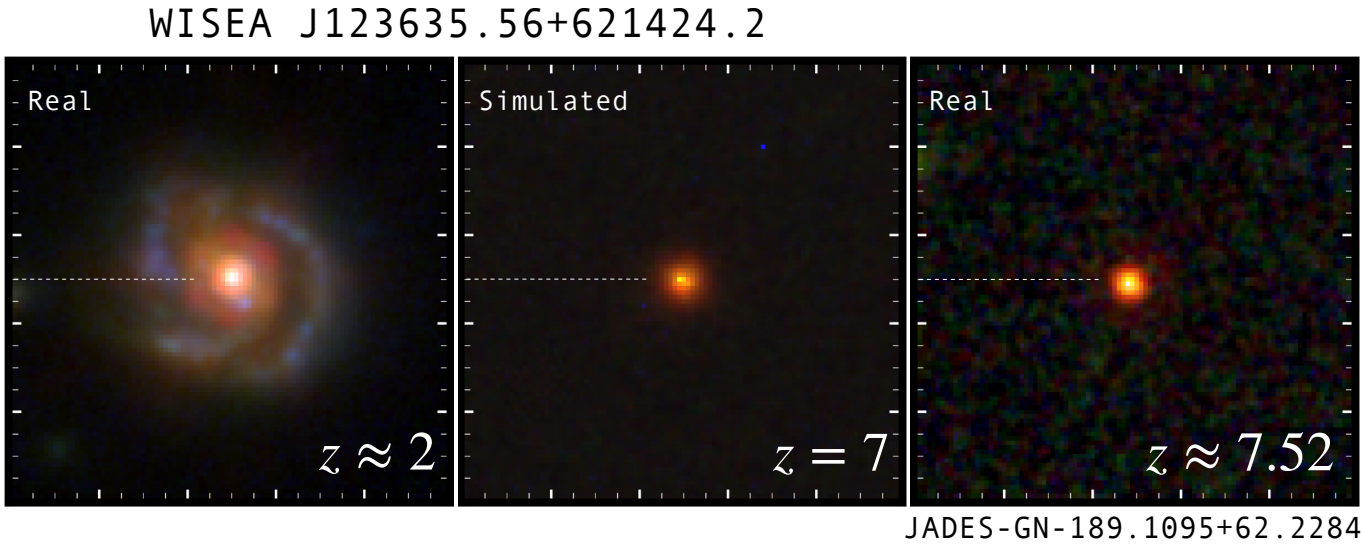

Figure 5. Visual demonstration of cosmological surface-brightness dimming and its impact on the host galaxy. **Left:** the real *Saguaro* (WISEA J123635.56+621424.2) observed at $z = 2.0145$. **Center:** the same galaxy artificially redshifted to $z = 7$ using the FERENGI prescription (M. Barden et al. 2008). **Right:** A representative LRD at comparable redshift from P. Rinaldi et al. (2024). All cutouts are $3'' \times 3''$. The toy experiment demonstrates how the host galaxy becomes increasingly suppressed in its outskirts, while the central regions remain detectable, mirroring the effect observed in LRDs. For these RGB images, we make use of F090W, F277W, and F444W.

may be biased, and a larger sample will be required to robustly confirm these findings.

Although the extended emission revealed in the stacked images is smaller than the ≈ 4–6 kpc hosts identified at $z \approx 2$, it is broadly consistent with the expected size evolution of galaxies. According to A. Genin et al. (2025), disk sizes roughly double between $z \approx 5$ and $z \approx 2$, implying that the compact high-redshift structures we observe could naturally evolve into the more extended hosts seen around systems like *the Saguaro* at later times. This strengthens the case for a physical connection between canonical LRDs and their potential lower-z analogs.

3.2. *The LRD visibility with redshift*

To further investigate the idea that our view of LRDs at high redshift may be biased, we develop a simple analytic model of surface brightness dimming to quantify how much of a LRD's extended host galaxy becomes undetectable at progressively higher redshifts. We assume the host follows a circular exponential light profile with a central surface brightness I_0 and scale radius R_s:

$$I(R) = I_0 \exp\left(-\frac{R}{R_s}\right) , \tag{1}$$

where $I(R)$ is the intrinsic surface brightness at galactocentric radius R. The total integrated luminosity of the host is then $L_{\rm host} = 2\pi I_0 R_s^2$.

Due to cosmological surface brightness dimming, the observed surface brightness is reduced by a factor of $(1+z)^4$ (R. C. Tolman 1930). We define the maximum detectable radius $R_{\rm max}$ at which the observed SB equals the detection limit $I_{\rm lim}$:

$$R_{\rm max}(z) = R_s \ln\left(\frac{I_0}{I_{\rm lim}(1+z)^4}\right) . \tag{2}$$

This expression requires the argument of the logarithm is larger than 1, which implies $I_0 > I_{\rm lim}(1+z)^4$. Within $R_{\rm max}$, the fraction of the total host light that remains detectable is computed as:

$$f_{\rm det}(z) = 1 - \left(1 + \frac{R_{\rm max}(z)}{R_s}\right) \exp\left(-\frac{R_{\rm max}(z)}{R_s}\right) . \tag{3}$$

The fraction lost is then $f_{\rm lost}(z) = 1 - f_{\rm det}(z)$.

To test this simple model, we adopt the following reference values, motivated by observed LRD properties and JWST detection thresholds: $I_0 = 100\, L_\odot\, {\rm pc}^{-2}$ (central surface brightness of the host), $R_s = 1.2$ kpc (scale radius, e.g. $\approx 0.2''$ at z = 7), and $I_{\rm lim} = 0.0079\, L_\odot\, {\rm pc}^{-2}$ (corresponding to $\mu \approx 28.5$ mag/arcsec^2 in the rest-UV).

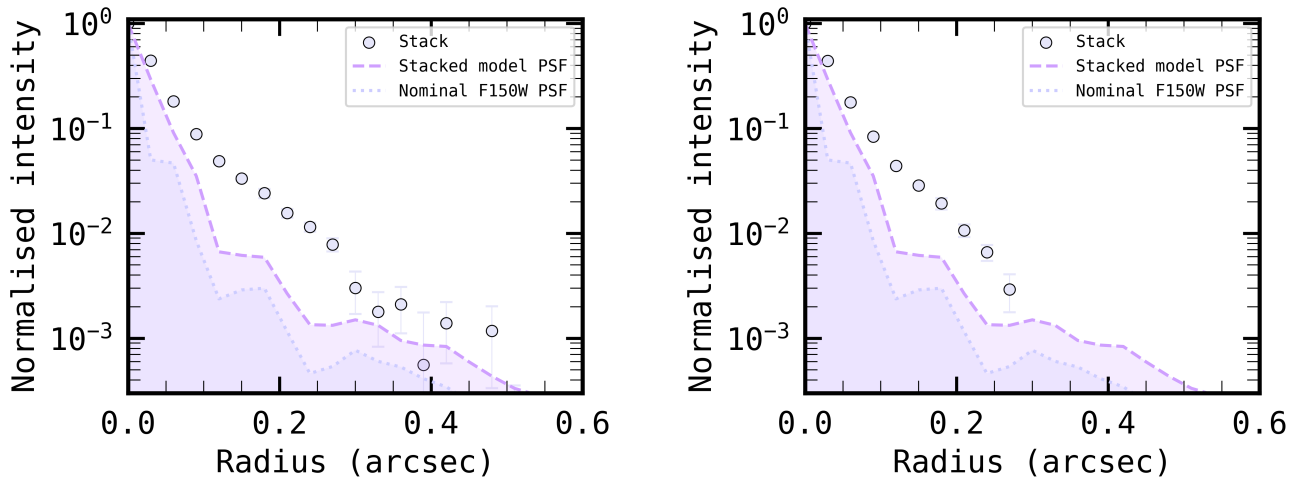

Figure 6. Left: Radial profile of the stacked image of 99 photometrically selected LRDs from P. Rinaldi et al. (2024) in the rest-frame UV (1500–2000 Å). **Right:** Same as on the left, but with the background artificially elevated to the highest level that does not cause the surrounding region to become strongly negative. To emphasize the extended nature of the stacked UV profile of the LRDs, we note that our simulated stacked PSF was constructed using a spatial offset of 1 pixel (≈ 30 mas for the NIRCam short wavelength channel), which is significantly larger (≈ 6×) than the typical internal astrometric scatter in the JADES images, thus representing an upper limit on the observed stacked PSF size. Altogether, this experiment reveals that the radial profile of the stacked LRDs declines less steeply than expected, suggesting that an extended structure may lie hidden beneath the observational noise.

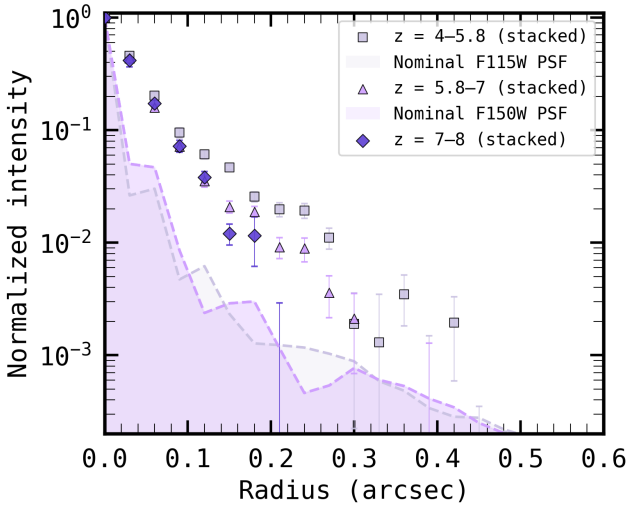

Figure 7. Radial profiles of the stacked rest-frame UV (1500–2000 Å) images of photometrically selected LRDs from P. Rinaldi et al. (2024), shown in redshift bins. For comparison, the nominal PSFs are overplotted: F115W for $z \approx 4$–5.8 and F150W for $z \approx 5.8$–8. A slight increase in radial extent is observed when moving from the highest to the lowest redshift bin.

The typical value for I_0 was taken from, e.g., S. Tacchella et al. (2015), for $z = 2$. We compute the lost light fraction for redshifts $z = 2$, 5, 7, and 9. The results are summarized in Table 2. If we also account for the observed redshift evolution of galaxy sizes (e.g., $R_s \propto (1+z)^{-m}$; K. Ormerod et al. 2024; A. Genin et al. 2025), the maximum detectable radius $R_{\rm max}$ would shrink significantly in physical units, further compounding the loss of extended light at high redshift.

Table 2. Surface Brightness Dimming Effects

z	$R_{\rm max}$ [kpc]	$f_{\rm det}$	$f_{\rm lost}$
2	5.59	0.914	0.086
5	2.73	0.664	0.336
7	1.35	0.311	0.689
9	0.28	0.024	0.976

These results show that, even for relatively compact and moderately bright host galaxies, surface brightness dimming can significantly limit the detection of extended components at high redshift. By $z \gtrsim 7$, more than two-thirds of the host light is lost to cosmological dimming, consistent with the observed compact morphologies of LRDs in JWST imaging. This calculation agrees with the model by F. Pacucci & A. Loeb (2025), which proposed that, at $z \gtrsim 8$, the observability of LRDs is significantly suppressed by the cosmological surface brightness dimming. Our results are also consistent with the recent findings of J.-B. Billand et al. (2025).

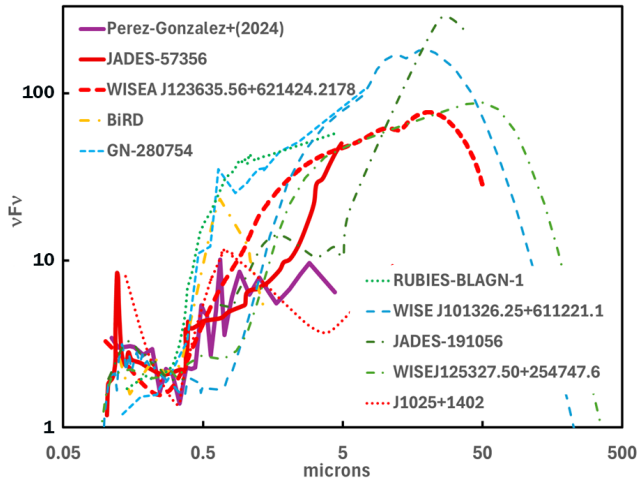

Figure 8. Comparison canonical LRDs with the nuclear SEDs for several relatively low-redshift LRD analogs. The heavy solid lines show: (1) the average SED from P. G. Pérez-González et al. (2024); and (2) the reddest example from the same paper, JADES-57356. WISEA J123635.56+621424.2 (i.e., *the Saguaro* discussed throughout this paper) is the heavy dashed line (the AGN portion only). The others are BiRD from F. Loiacono et al. (2025), GN-280754 I. Juodžbalis et al. (2024); RUBIES-BLAGN-1 from B. Wang et al. (2024); WISE J101326.25+611221.1, a particularly luminous blu-DOG identified by Y. Toba et al. (2018); JADES 191056 G. Barro et al. (2024a); WISE J125327.50+254747 G. Li et al. (2025); and J1025+1402 from X. Lin et al. (2025).

The surface brightness dimming for high redshift LRDs is strong enough that we cannot tell if they are truly isolated point-like sources or if they are the nuclei of more extended galaxies.

4. LOW-REDSHIFT ANALOGS: HOW TYPICAL IS *THE SAGUARO*?

It is not yet clear how to trace LRDs to lower redshifts. For example, a ground-based survey over 3.11 deg^2 by Y. Ma et al. (2025) reports a one-order-of-magnitude drop in the LRD number density from $z > 4$ to $1.7 < z < 2.7$, consistent with D. D. Kocevski et al. (2024) and V. Kokorev et al. (2024). In contrast, a wide-area *Euclid* survey over 63 deg^2 finds numerous LRD candidates at $z < 4$, with number densities increasing down to $z \approx 1.5$–2.5 before declining at lower redshifts (L. Bisigello Euclid Collaboration). These conflicting results likely reflect fundamental differences in selection methodology.

For instance, Y. Ma et al. (2025) adopt a stringent cut, $(m_{\rm PSF} - m_{\rm CModel}) < 0.016$, highly sensitive to faint, extended halos. Conversely, the *Euclid* team uses a peak–surface-brightness criterion, $\mu_{\rm max} - m_{\rm pointlike} < -2.6$ mag arcsec^{-2}, which remains sensitive to moderate halos but is somewhat less punitive than the criterion from Y. Ma et al. (2025). The importance of selection criteria is made clear in this section, where we discuss half a dozen proposed low redshift analogs, all of which appear to have the signature V-shaped SED (or one close to this shape) and are compact, but as summarized in Figure 8 exhibit a wide range of behavior in the longer-wavelength infrared.

As a baseline, X. Lin et al. (2025) identified three LRD analogs at $z \approx 0.1$ in the SDSS database, across 9,376 deg^2. They note the sample is likely incomplete due to SDSS's biases against LRDs. Moreover, their selection criteria also differ from those of both Y. Ma et al. (2025) and L. Bisigello (Euclid Collaboration). Nonetheless, they have demonstrated for the first time that low redshift analogs *actually exist*!

The examples found by X. Lin et al. (2025) must be rare, given the very large parent sample. In fact, canonical LRDs known from existing studies are rare at redshifts less than 4 (e.g., D. D. Kocevski et al. 2024; V. Kokorev et al. 2024; Y. Ma et al. 2025). To understand their evolution we need to identify what they become as they age beyond this point. Of course, it is conceivable that they morph into perfectly ordinary-appearing galaxies (F. M. Khan et al. 2025), in which case following their evolution will be difficult. We take the more optimistic stance that their evolutionary products will share many of their properties, subtly modified by the evolution.

We have argued that LRDs could lie in compact, low surface brightness host galaxies at high redshifts. By z $\approx$ 2, compared with z $\approx$ 5, we can expect the hosts to double in diameter and to have much higher surface densities of star formation (e.g., A. Genin et al. 2025), making the hosts more prominent than for the classic LRDs. We can also expect their interstellar medium (ISM) metallicities to have increased, possibly making their already dust-embedded characteristics even more pronounced.

With these considerations in mind, we list some sibling candidates and show their SEDs in Figure 8, along with both an average SED for canonical LRDs and the SED of the reddest LRD known from P. G. Pérez-González et al. (2024). All of these proposed "siblings" have a flattening of their SEDs short of 1 μm, and some have the signature "V-shape". Whether the rest show this shape intrinsically depends on the amount of reddening one needs to correct in the observations. Given the increase in dust expected at the lower redshifts, we do not reject any proposed siblings on the basis of a flat, rather than rising, UV SED.

In addition to *the Saguaro* (WISEA J123635.56+621424.2), in Figure 8, we show SEDs of:

- The Big Red Dot (BiRD) at $z = 2.33$ (F. Loiacono et al. 2025). It has a unique SED that turns over toward longer wavelengths near 0.5 μm.
- GN 280754 at $z = 2.26$, advertised as *the Rosetta stone of JWST-discovered AGN* by I. Juodžbalis et al. (2024).
- RUBIES-BLAGN-1 at $z = 3.10$. B. Wang et al. (2025a) have modeled the SED of this source in detail, finding that the UV is dominated by hot stars that are moderately obscured, with the turnup in the UV reflecting the result of dereddening.
- J101326.25+611220.1 at $z = 3.703$ (Y. Toba et al. 2018. In this regard, A. Noboriguchi et al. (2023) called attention to the possible relation of DOGs discovered with Spitzer (e.g., A. Dey et al. 2008) and LRDs, particularly for those DOGs with blue excesses (namely, Blue HotDOGs; e.g., R. J. Assef et al. 2016; A. Noboriguchi et al. 2022). This galaxy is an excellent example.
- JADES-GS-191056 at $z = 3.139$ (G. Barro et al. 2024b). In the short wavelength JWST/NIRCam bands, this source is extended with a complex morphology, suggesting a possible interaction or other disturbance to its host galaxy as found for a significant number of LRDs by P. Rinaldi et al. (2024).
- WISE J125327.50+254747.6, at $z = 0.485$ (G. Li et al. 2025). The compactness of this source is demonstrated in the imaging of R. C. McGurk et al. (2015). This is a Hot DOG, but at an exceptionally low redshift, and with properties suggesting they represent a transient stage of evolution (G. Li et al. 2025).
- J1025+1402, one of three sources found in SDSS by X Lin et al. (2025) at z $\approx$ 0.1 that show very close resemblance to canonical LRDs. This similarity is apparent in the close match of its SED to the average for canonical LRDs from P. G. Pérez-González et al. (2024) and shows that these sources are uniquely important for probing what are possibly *real* LRDs
- R. Lin et al. (2024) call attention to some resemblances betweeen LRDs and compact Green Pea AGNs. However the infrared properties of these candidates need to be better constrained before we can classify them with the other LRD siblings.

The following list presents illustrative examples; other LRD siblings likely exist with similar characteristics:

- There are a number of galaxies related to J123635.56+621424.2 with similar SEDs and point-like HST images, e.g. IRBG2, IRBG4, IRBG5, and IRBG7 in the notation of J. L. Donley et al. (2010) (their Table 2). These also have extended host galaxies that would fade in surface brightness and probably not be prominent at the redshifts of classic LRDs.
- Some Type II quasars have appropriate SEDs (B. Wang et al. 2025b); better high resolution imaging is needed to confirm that they are sufficiently compact.
- With two entries already in the list above, it is clear that evaluation among BluDOGs and just DOGs is likely to reveal additional candidates (A. Noboriguchi et al. 2022).

The variety and abundance of these "siblings" is promising, indicating that a more thorough search may reveal additional evolutionary counterparts of classical LRDs at later cosmic time.

5. DISCUSSION AND CONCLUSIONS

LRDs have become perhaps the most intensively studied high redshift discovery with JWST. Two of their salient characteristics are: (1) point-like morphology (e.g., I. Labbé et al. 2023; J. F. W. Baggen et al. 2024; J. Matthee et al. 2024); and (2) high number densities, perhaps a few percent of population of galaxies at z > 5 (V. Kokorev et al. 2024), but dropping steeply from $z = 4$ to $z = 2$ (Y. Ma et al. 2025). These behaviors raise a fundamental question: if they lack detectable host galaxies, where did they come from, and, as phrased by F. M. Khan et al. (2025), *where have all the LRDs gone?* We address the second question first.

There must be some form(s) of galaxy that includes the descendents of the LRDs. Identifying this evolutionary phase requires understanding which types of galaxies resemble LRDs and tracing them back to the redshifts where LRDs were more prevalent. Since it is unclear what direction their evolution will take, it is important to identify a range of possible descendants. Toward that end, we have presented a detailed analysis of the characteristics of *the Saguaro*. Through a detailed AGN–host image decomposition and spatial analysis of its NIRSpec spectrum, we reveal a "V-shaped" SED arises from its nuclear region. Although the nucleus lies within a face-on spiral galaxy that is clearly visible at $z \approx 2$,

we prove, using a toy experiment, that the surrounding galaxy would be virtually undetectable if observed at $z = 7$ due to cosmological surface brightness dimming. This would leave the nucleus entirely "naked", revealing a very compact, heavily dust-embedded AGN with a characteristic "V-shaped" SED, typical of LRDs. That is, it would readily be identified as a canonical LRD using the limited spectral range provided by the NIRCam filter set at high redshifts. At the moment we are observing it ($z \approx 2$), it is a star-forming ULIRG with a strong sub-mm output. Nonetheless, when this fades (in a few tens of Myr), it will resemble LRDs even more closely. Thus, it can take its place among the menagerie of objects at redshifts of 2–4 that have been suggested to be related to LRDs.

The disappearance of the host of *the Saguaro* at high redshifts led us to look in more detail for the potential presence of undetected hosts around canonical LRDs. By stacking the images of the full sample of 99 LRDs from P. Rinaldi et al. (2024), we found significant excess emission extending to a radius of $0.2''$, or $\approx$ 2–3 kpc in diameter. That is, on average canonical LRDs at high redshift tend to lie within an enveloping galaxy that is not apparent at typical imaging depths due to surface brightness dimming.

Finally, we did an analysis of the general expected effects of surface brightness dimming on LRD hosts as a function of redshift. This shows that most of the host galaxy signal slips below typical detection limits by $z = 7$ and hosts are virtually undetectable by $z = 9$. We conclude that current measurements are agnostic as to whether LRDs form in isolation or represent the nuclei of extended host galaxies. This ambiguity likely stems from observational biases: at high redshift, we may be seeing only the bright core, *the tip of the iceberg*, while more extended components either remain undetected due to resolution and sensitivity limits or are still in the process of assembling.

In light of the existence of objects (i.e., LRDs) showing a "V-shaped" SEDs from $z \approx 8$–9 down to $z \approx 0.1$, it becomes clear that the "LRD phase" is not exclusive to the early Universe, but may represent a specific evolutionary stage that galaxies undergo under certain physical conditions. Their compact, red appearance may not indicate a distinct class of objects, but rather a transient and observationally biased view of systems that are more extended and complex than they initially appear, with the visible component likely tracing the peak of interaction between the central SMBH and its host galaxy.

The launch of JWST has undoubtedly transformed our view of the early Universe, greatly enhancing our ability to observe high-z galaxies and fundamentally challenging several aspects of pre-JWST galaxy formation and evolution paradigms. The systematic discovery of LRDs has raised numerous questions about the early growth of black holes and the co-evolution of galaxies and SMBHs at high redshift. While uncovering their true nature is fundamental, it is equally important to investigate what these sources may evolve into at later epochs, as this provides crucial insight into galaxy evolution across cosmic time. In this context, *the Saguaro* may serve as a valuable link, and future high-resolution spectroscopic follow-up will be essential to further study the nature of its core.

ACKNOWLEDGMENTS

The authors thank Xiaohui Fan, Xiaojing Lin, Camilla Pacifici, Marianna Annunziatella, Claudia Scarlata, Luis C. Ho, and Pablo G. Pérez-González for valuable discussions.

This work is based on observations made with the NASA/ESA/CSA JWST. The data were obtained from the Mikulski Archive for Space Telescopes (MAST) at the Space Telescope Science Institute, which is operated by the Association of Universities for Research in Astronomy, Inc., under NASA contract NAS 5-03127 for JWST. These observations are associated with JWST programs GTO #1181 and GO #1895.

The authors acknowledge the FRESCO team led by PI P. Oesch for developing their observing program with a zero-exclusive-access period. Processing for the JADES NIRCam data release was performed on the lux cluster at the University of California, Santa Cruz, funded by NSF MRI grant AST 1828315. Also based on observations made with the NASA/ESA Hubble Space Telescope obtained from the Space Telescope Science Institute, which is operated by the Association of Universities for Research in Astronomy, Inc., under NASA contract NAS 526555. The data presented in this article were obtained from MAST at the Space Telescope Science Institute. The specific observations analyzed can be accessed via DOI: 10.17909/gdyc-7g80, 10.17909/T91019, 10.17909/8tdj-8n28.

The authors acknowledge use of the lux supercomputer at UC Santa Cruz, funded by NSF MRI grant AST 1828315.

AJB acknowledges funding from the "FirstGalaxies" Advanced Grant from the European Research Council (ERC) under the European Union's Horizon 2020 research and innovation programme (Grant agreement No. 789056)

BER acknowledges support from the NIRCam Science Team contract to the University of Arizona, NAS5-02015, and JWST Program 3215.

The research of CCW is supported by NOIRLab, which is managed by the Association of Universities for Research in Astronomy (AURA) under a cooperative agreement with the National Science Foundation.

SC acknowledges support by European Union's HE ERC Starting Grant No. 101040227 - WINGS.

YZ, ZJ, BDJ, CNAW, and PL gratefully acknowledge JWST/NIRCam contract to the University of Arizona NAS5-02015.

The work of GHR and PL was also supported by grant 80NSSC18K0555, from NASA Goddard Space Flight Center to the University of Arizona.

SA acknowledges support from the JWST Mid-Infrared Instrument (MIRI) Science Team Lead, grant 80NSSC18K0555, from NASA Goddard Space Flight Center to the University of Arizona.

RM, FDE acknowledge support by the Science and Technology Facilities Council (STFC), by the ERC through Advanced Grant 695671 "QUENCH", and by the UKRI Frontier Research grant RISEandFALL. RM also acknowledges funding from a research professorship from the Royal Society.

LB acknowledges financial support from the Inter-University Institute for Data Intensive Astronomy (IDIA), a partnership of the University of Cape Town, the University of Pretoria and the University of the Western Cape, and from the South African Department of Science and Innovation's National Research Foundation under the ISARP RADIOMAP+ Joint Research Scheme (DSI-NRF Grant Number 150551) and the CPRR HIPPO Project (DSI-NRF Grant Number SRUG22031677). CJEG acknowledges the financial assistance of the South African Radio Astronomy Observatory (SARAO) (www.sarao.ac.za).

APPENDIX

We present the results of the AGN–host image decomposition using both HST and JWST/NIRCam data in Table 3. We present the data, model, and residual images in $1.5'' \times 1.5''$ cutouts in Figure 9. We report the residuals in the ΔFlux metric, which quantifies the percentage difference between the model (AGN + host) and the observed flux within the same aperture. This quantity is evaluated across circular apertures with radii ranging from $0.1''$ to $0.6''$. Across all HST and JWST bands, the residual flux after AGN-host decomposition remains modest, with average values around 6–7% and typically below 10% at all apertures, thus leading to a negligible impact on the photometric measurements for both host and AGN.

Table 3. Flux densities of the AGN and host galaxy across HST and JWST filters.

Band	**AGN Flux (μJy)**	**Host Flux (μJy)**
F435W	0.42	0.54
F606W	0.42	0.84
F775W	0.44	1.23
F814W	0.47	1.45
F090W	0.47	2.02
F105W	0.82	2.94
F115W	0.82	4.80
F125W	1.05	5.68
F140W	1.68	7.42
F150W	2.17	9.03
F160W	2.51	8.88
F182M	3.44	13.10
F200W	4.97	15.30
F210M	5.15	16.33
F277W	12.02	23.48
F335M	23.33	30.48
F356W	27.29	33.00
F410M	44.46	37.78
F444W	56.49	41.57

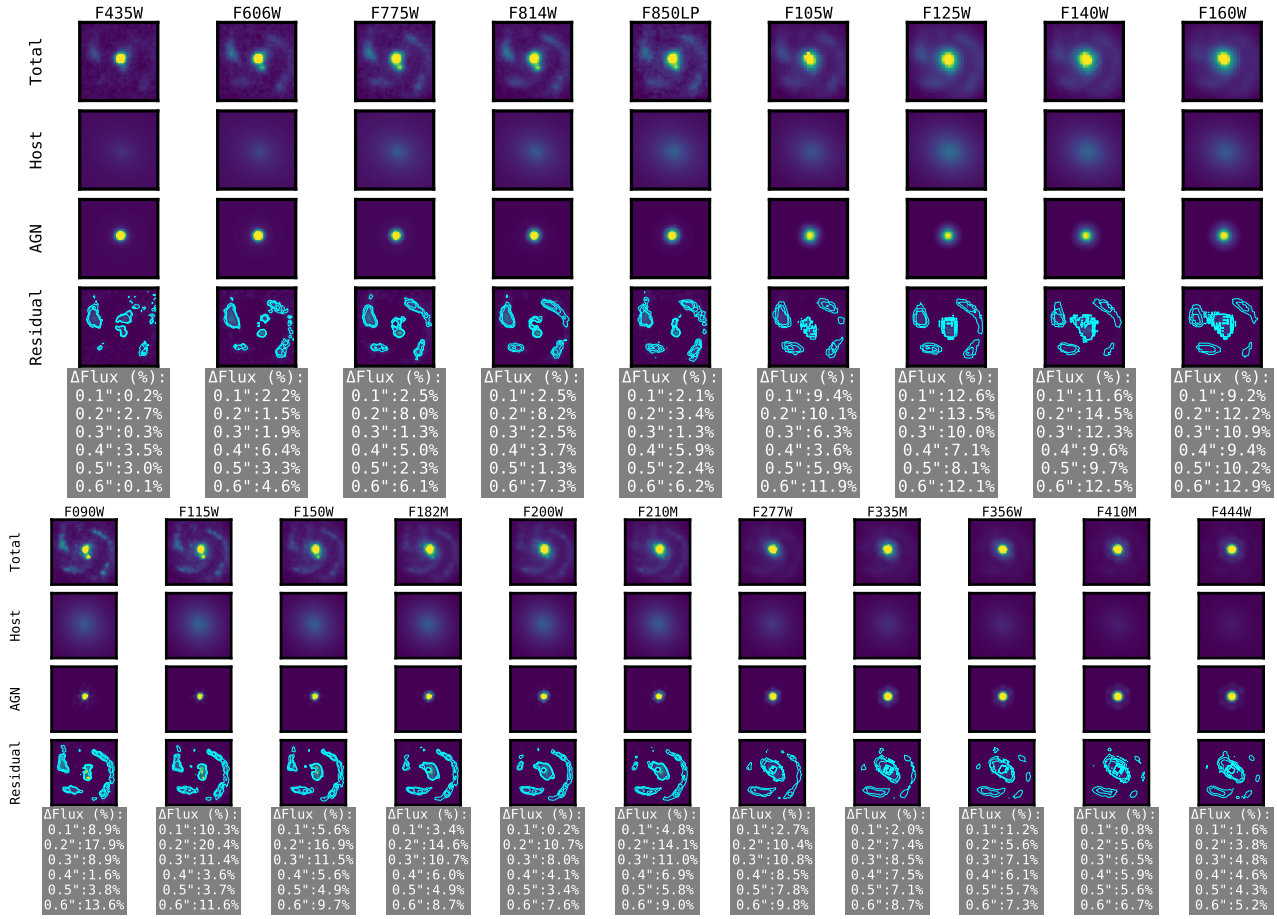

Figure 9. AGN-host image decomposition for HST (**top**) and NIRCam (**bottom**). Each cutout is $1.5'' \times 1.5''$. The first row shows the original image (total), followed by the host and AGN model components in the second and third rows, respectively. The final row displays the residuals, with overlaid contours highlighting the residual structures. All cutouts are shown using the same scale as the original image in each band.

Facilities: *Chandra*, *HST*, *JWST*.

Software: Astropy (Astropy Collaboration et al. 2022), Bagpipes (A. C. Carnall et al. 2019), MSAEXP (G. Brammer 2023) NumPy (C. R. Harris et al. 2020), pandas (T. p. d. team 2024) Photutils (L. Bradley et al. 2016), TOPCAT (M. Taylor 2022), CIAO (A. Fruscione et al. 2006), XSpec (K. Arnaud et al. 1999), STPSF (M. D. Perrin et al. 2014).

REFERENCES

Akins, H. B., Casey, C. M., Lambrides, E., et al. 2024, doi: 10.48550/arXiv.2406.10341

Alexander, D. M., Bauer, F. E., Chapman, S. C., et al. 2005, The Astrophysical Journal, 632, 736, doi: 10.1086/444342

Ananna, T. T., Bogdán, A., Kovács, O. E., Natarajan, P., & Hickox, R. C. 2024, The Astrophysical Journal Letters, Volume 969, Issue 1, id.L18, 10 pp., 969, L18, doi: 10.3847/2041-8213/ad5669

Arnaud, K., Dorman, B., & Gordon, C. 1999, Astrophysics Source Code Library, ascl:9910.005. https://ui.adsabs.harvard.edu/abs/1999ascl.soft10005A/abstract

Assef, R. J., Walton, D. J., Brightman, M., et al. 2016, The Astrophysical Journal, 819, 111, doi: 10.3847/0004-637X/819/2/111

Astropy Collaboration, Price-Whelan, A. M., Lim, P. L., et al. 2022, The Astrophysical Journal, 935, 167, doi: 10.3847/1538-4357/ac7c74

Auge, C., Sanders, D., Treister, E., et al. 2023, The Astrophysical Journal, 957, 19, doi: 10.3847/1538-4357/acf21a

Baggen, J. F. W., van Dokkum, P., Brammer, G., et al. 2024, doi: 10.48550/arXiv.2408.07745

Barchiesi, L., Vignali, C., Pozzi, F., et al. 2024, Astronomy and Astrophysics, 685, A141, doi: 10.1051/0004-6361/202245288

Barden, M., Jahnke, K., & Häußler, B. 2008, The Astrophysical Journal Supplement Series, Volume 175, Issue 1, pp. 105-115 (2008)., 175, 105, doi: 10.1086/524039

Barro, G., Pérez-González, P. G., Kocevski, D. D., et al. 2024a, The Astrophysical Journal, 963, 128, doi: 10.3847/1538-4357/ad167e

Barro, G., Perez-Gonzalez, P. G., Kocevski, D. D., et al. 2024b, arXiv e-prints, arXiv:2412.01887, doi: 10.48550/arXiv.2412.01887

Billand, J.-B., Elbaz, D., Gentile, F., et al. 2025, arXiv e-prints, arXiv:2507.04011, doi: 10.48550/arXiv.2507.04011

Bisigello (Euclid Collaboration)), L., Bisigello, L., Rodighiero, G., et al. 2025, arXiv e-prints, arXiv:2503.15323, doi: 10.48550/arXiv.2503.15323

Bohn, T., Inami, H., Diaz-Santos, T., et al. 2023, The Astrophysical Journal, 942, L36, doi: 10.3847/2041-8213/acab61

Bongiorno, A., Maiolino, R., Brusa, M., et al. 2014, Monthly Notices of the Royal Astronomical Society, 443, 2077, doi: 10.1093/mnras/stu1248

Borys, C., Smail, I., Chapman, S. C., et al. 2005, The Astrophysical Journal, Volume 635, Issue 2, pp. 853-863., 635, 853, doi: 10.1086/491617

Bradley, L., Sipocz, B., Robitaille, T., et al. 2016, Astrophysics Source Code Library, ascl:1609.011. https://ui.adsabs.harvard.edu/abs/2016ascl.soft09011B

Brammer, G. 2023, Zenodo, doi: 10.5281/zenodo.7299500

Brammer, G. B., van Dokkum, P. G., & Coppi, P. 2008, The Astrophysical Journal, 686, 1503, doi: 10.1086/591786

Brown, M. J. I., Moustakas, J., Smith, J.-D. T., et al. 2014, The Astrophysical Journal Supplement Series, 212, 18, doi: 10.1088/0067-0049/212/2/18

Calvi, V., Stiavelli, M., Bradley, L., Pizzella, A., & Kim, S. 2014, The Astrophysical Journal, 796, 102, doi: 10.1088/0004-637X/796/2/102

Calzetti, D., Armus, L., Bohlin, R. C., et al. 2000, The Astrophysical Journal, 533, 682, doi: 10.1086/308692

Carnall, A. C., McLure, R. J., Dunlop, J. S., et al. 2019, Monthly Notices of the Royal Astronomical Society, 490, 417, doi: 10.1093/mnras/stz2544

Casey, C. M., Akins, H. B., Finkelstein, S. L., et al. 2025, arXiv e-prints, arXiv:2505.18873, doi: 10.48550/arXiv.2505.18873

Cash, W. 1979, The Astrophysical Journal, 228, 939, doi: 10.1086/156922

Chen, C.-H., Ho, L. C., Li, R., & Inayoshi, K. 2025a, arXiv e-prints, arXiv:2505.03183, doi: 10.48550/arXiv.2505.03183

Chen, C.-H., Ho, L. C., Li, R., & Zhuang, M.-Y. 2025b, The Astrophysical Journal, Volume 983, Issue 1, id.60, 25 pp., 983, 60, doi: 10.3847/1538-4357/ada93a

Cleri, N. J., Yang, G., Papovich, C., et al. 2023, The Astrophysical Journal, 948, 112, doi: 10.3847/1538-4357/acc1e6

de Graaff, A., Rix, H.-W., Naidu, R. P., et al. 2025a, arXiv e-prints, arXiv:2503.16600, doi: 10.48550/arXiv.2503.16600

de Graaff, A., Brammer, G., Weibel, A., et al. 2025b, Astronomy and Astrophysics, 697, A189, doi: 10.1051/0004-6361/202452186

Del Moro, A., Alexander, D. M., Bauer, F. E., et al. 2016, Monthly Notices of the Royal Astronomical Society, 456, 2105, doi: 10.1093/mnras/stv2748

D'Eugenio, F., Cameron, A. J., Scholtz, J., et al. 2024, doi: 10.48550/arXiv.2404.06531

Dey, A., Soifer, B. T., Desai, V., et al. 2008, The Astrophysical Journal, 677, 943, doi: 10.1086/529516

Dimauro, P., Huertas-Company, M., Daddi, E., et al. 2019, Monthly Notices of the Royal Astronomical Society, 489, 4135, doi: 10.1093/mnras/stz2421

Dojčinović, I., Kovačević-Dojčinović, J., & Popović, L. A. 2023, Advances in Space Research, 71, 1219, doi: 10.1016/j.asr.2022.04.041

Donley, J. L., Rieke, G. H., Alexander, D. M., Egami, E., & Pérez-González, P. G. 2010, The Astrophysical Journal, 719, 1393, doi: 10.1088/0004-637X/719/2/1393

Duras, F., Bongiorno, A., Ricci, F., et al. 2020, Astronomy and Astrophysics, 636, A73, doi: 10.1051/0004-6361/201936817

Efstathiou, A., Pearson, C., Farrah, D., et al. 2014, Monthly Notices of the Royal Astronomical Society, 437, L16, doi: 10.1093/mnrasl/slt131

Eisenstein, D. J., Willott, C., Alberts, S., et al. 2023a, doi: 10.48550/arXiv.2306.02465

Eisenstein, D. J., Johnson, B. D., Robertson, B., et al. 2023b, doi: 10.48550/arXiv.2310.12340

Ferruit, P., Jakobsen, P., Giardino, G., et al. 2022, Astronomy and Astrophysics, 661, A81, doi: 10.1051/0004-6361/202142673

Feuillet, L. M., Meléndez, M., Kraemer, S., et al. 2024, The Astrophysical Journal, 968, 91, doi: 10.3847/1538-4357/ad47bb

Fisher, D. B., & Drory, N. 2008, The Astronomical Journal, 136, 773, doi: 10.1088/0004-6256/136/2/773

Fruscione, A., McDowell, J. C., Allen, G. E., et al. 2006, Observatory Operations: Strategies, Processes, and Systems, 6270, 62701V, doi: 10.1117/12.671760

Furtak, L. J., Zitrin, A., Plat, A., et al. 2023, The Astrophysical Journal, 952, 142, doi: 10.3847/1538-4357/acdc9d

Förster Schreiber, N. M., Genzel, R., Lutz, D., & Sternberg, A. 2003, The Astrophysical Journal, 599, 193, doi: 10.1086/379097

Gardner, J. P., Mather, J. C., Abbott, R., et al. 2023, Publications of the Astronomical Society of the Pacific, 135, 068001, doi: 10.1088/1538-3873/acd1b5

Gehrz, R. D., Roellig, T. L., Werner, M. W., et al. 2007, Review of Scientific Instruments, 78, 011302, doi: 10.1063/1.2431313

Genin, A., Shuntov, M., Brammer, G., et al. 2025, eprint arXiv:2505.21622, arXiv:2505.21622, doi: 10.48550/arXiv.2505.21622

Gilli, R., Vignali, C., Mignoli, M., et al. 2010, Astronomy and Astrophysics, 519, A92, doi: 10.1051/0004-6361/201014039

Gilli, R., Norman, C., Vignali, C., et al. 2014, Astronomy and Astrophysics, 562, A67, doi: 10.1051/0004-6361/201322892

Gillman, S., Pye, J. P., Alonso-Herrero, A., et al. 2025, doi: 10.48550/arXiv.2501.11491

Greene, J. E., Seth, A., Kim, M., et al. 2016, The Astrophysical Journal, 826, L32, doi: 10.3847/2041-8205/826/2/L32

Greene, J. E., Labbe, I., Goulding, A. D., et al. 2024, The Astrophysical Journal, 964, 39, doi: 10.3847/1538-4357/ad1e5f

Hainline, K. N., Maiolino, R., Juodzbalis, I., et al. 2024, doi: 10.48550/arXiv.2410.00100

Hanish, D. J., Capak, P., Teplitz, H. I., et al. 2015, The Astrophysical Journal Supplement Series, Volume 217, Issue 1, article id. 17, <NUMPAGES>6</NUMPAGES> pp. (2015)., 217, 17, doi: 10.1088/0067-0049/217/1/17

Harikane, Y., Zhang, Y., Nakajima, K., et al. 2023, The Astrophysical Journal, 959, 39, doi: 10.3847/1538-4357/ad029e

Harris, C. R., Millman, K. J., van der Walt, S. J., et al. 2020, Nature, 585, 357, doi: 10.1038/s41586-020-2649-2

Harrison, F. A., Craig, W. W., Christensen, F. E., et al. 2013, The Astrophysical Journal, 770, 103, doi: 10.1088/0004-637X/770/2/103

Hodge, J. A., Smail, I., Walter, F., et al. 2019, The Astrophysical Journal, 876, 130, doi: 10.3847/1538-4357/ab1846

Häußler, B., Bamford, S. P., Vika, M., et al. 2013, Monthly Notices of the Royal Astronomical Society, 430, 330, doi: 10.1093/mnras/sts633

Jakobsen, P., Ferruit, P., Alves de Oliveira, C., et al. 2022, Astronomy and Astrophysics, 661, A80, doi: 10.1051/0004-6361/202142663

Juodžbalis, I., Ji, X., Maiolino, R., et al. 2024, Monthly Notices of the Royal Astronomical Society, 535, 853, doi: 10.1093/mnras/stae2367

Kalita, B. S., Silverman, J. D., Daddi, E., et al. 2024, The Astrophysical Journal, 960, 25, doi: 10.3847/1538-4357/acfee4

Khan, F. M., Davis, B. L., Macciò, A. V., & Holley-Bockelmann, K. 2025, The Astrophysical Journal, 986, L1, doi: 10.3847/2041-8213/adda4c

Killi, M., Watson, D., Brammer, G., et al. 2023, doi: 10.48550/arXiv.2312.03065

Kocevski, D. D., Finkelstein, S. L., Barro, G., et al. 2024, doi: 10.48550/arXiv.2404.03576

Kokorev, V., Fujimoto, S., Labbe, I., et al. 2023, The Astrophysical Journal, 957, L7, doi: 10.3847/2041-8213/ad037a

Kokorev, V., Caputi, K. I., Greene, J. E., et al. 2024, The Astrophysical Journal, 968, 38, doi: 10.3847/1538-4357/ad4265

Kotilainen, J. K., Reunanen, J., Laine, S., & Ryder, S. D. 2000, Astronomy and Astrophysics, 353, 834. https://ui.adsabs.harvard.edu/abs/2000A&A...353..834K/abstract

Kriek, M., & Conroy, C. 2013, The Astrophysical Journal, 775, L16, doi: 10.1088/2041-8205/775/1/L16

Kroupa, P. 2001, Monthly Notices of the Royal Astronomical Society, 322, 231, doi: 10.1046/j.1365-8711.2001.04022.x

Labbé, I., van Dokkum, P., Nelson, E., et al. 2023, Nature, 616, 266, doi: 10.1038/s41586-023-05786-2

LaMassa, S., Farrow, I., Urry, C. M., et al. 2025, arXiv e-prints, arXiv:2501.14072, doi: 10.48550/arXiv.2501.14072

Li, G., Wu, J., Tsai, C.-W., et al. 2025, The Astrophysical Journal, 981, 104, doi: 10.3847/1538-4357/adabe3

Lin, R., Zheng, Z.-Y., Jiang, C., et al. 2024, doi: 10.48550/arXiv.2412.08396

Lin, X., Wang, F., Fan, X., et al. 2024, The Astrophysical Journal, 974, 147, doi: 10.3847/1538-4357/ad6565

Lin, X., Fan, X., Cai, Z., et al. 2025, arXiv e-prints, arXiv:2507.10659. https://ui.adsabs.harvard.edu/abs/2025arXiv250710659L/abstract

Liu, D., Daddi, E., Dickinson, M., et al. 2018, The Astrophysical Journal, 853, 172, doi: 10.3847/1538-4357/aaa600

Liu, F.-Y., Dai, Y. S., Omont, A., et al. 2024, The Astrophysical Journal, 964, 136, doi: 10.3847/1538-4357/ad24fe

Loiacono, F., Gilli, R., Mignoli, M., et al. 2025, eprint arXiv:2506.12141, arXiv:2506.12141, doi: 10.48550/arXiv.2506.12141

Lusso, E., & Risaliti, G. 2016, The Astrophysical Journal, 819, 154, doi: 10.3847/0004-637X/819/2/154

Lusso, E., Comastri, A., Vignali, C., et al. 2010, Astronomy and Astrophysics, 512, A34, doi: 10.1051/0004-6361/200913298

Ma, Y., Greene, J. E., Setton, D. J., et al. 2025, arXiv e-prints, arXiv:2504.08032, doi: 10.48550/arXiv.2504.08032

Maiolino, R., Scholtz, J., Curtis-Lake, E., et al. 2023, doi: 10.48550/arXiv.2308.01230

Maiolino, R., Risaliti, G., Signorini, M., et al. 2025, Monthly Notices of the Royal Astronomical Society, 538, 1921, doi: 10.1093/mnras/staf359

Maseda, M. V., de Graaff, A., Franx, M., et al. 2024, Astronomy and Astrophysics, 689, A73, doi: 10.1051/0004-6361/202449914

Matthee, J., Naidu, R. P., Brammer, G., et al. 2024, The Astrophysical Journal, 963, 129, doi: 10.3847/1538-4357/ad2345

Mazzolari, G., Gilli, R., Maiolino, R., et al. 2024, arXiv e-prints, arXiv:2412.04224, doi: 10.48550/arXiv.2412.04224

McGurk, R. C., Max, C. E., Medling, A. M., Shields, G. A., & Comerford, J. M. 2015, The Astrophysical Journal, 811, 14, doi: 10.1088/0004-637X/811/1/14

Murphy, K. D., & Yaqoob, T. 2009, Monthly Notices of the Royal Astronomical Society, 397, 1549, doi: 10.1111/j.1365-2966.2009.15025.x

Naidu, R. P., Oesch, P. A., Reddy, N., et al. 2017, The Astrophysical Journal, 847, 12, doi: 10.3847/1538-4357/aa8863

Noboriguchi, A., Inoue, A. K., Nagao, T., Toba, Y., & Misawa, T. 2023, The Astrophysical Journal, 959, L14, doi: 10.3847/2041-8213/ad0e00

Noboriguchi, A., Nagao, T., Toba, Y., et al. 2022, The Astrophysical Journal, 941, 195, doi: 10.3847/1538-4357/aca403

Oesch, P. A., Bouwens, R. J., Illingworth, G. D., Labbé, I., & Stefanon, M. 2018, The Astrophysical Journal, Volume 855, Issue 2, article id. 105, <NUMPAGES>12</NUMPAGES> pp. (2018)., 855, 105, doi: 10.3847/1538-4357/aab03f

Oesch, P. A., Brammer, G., Naidu, R. P., et al. 2023, Monthly Notices of the Royal Astronomical Society, 525, 2864, doi: 10.1093/mnras/stad2411

Oke, J. B., & Gunn, J. E. 1983, The Astrophysical Journal, 266, 713, doi: 10.1086/160817

Ormerod, K., Conselice, C. J., Adams, N. J., et al. 2024, Monthly Notices of the Royal Astronomical Society, 527, 6110, doi: 10.1093/mnras/stad3597

Pacucci, F., & Loeb, A. 2025, arXiv e-prints, arXiv:2506.03244, doi: 10.48550/arXiv.2506.03244

Pacucci, F., Nguyen, B., Carniani, S., Maiolino, R., & Fan, X. 2023, The Astrophysical Journal, 957, L3, doi: 10.3847/2041-8213/ad0158

Parlanti, E., Carniani, S., Übler, H., et al. 2024, Astronomy and Astrophysics, 684, A24, doi: 10.1051/0004-6361/202347914

Peng, C. Y., Ho, L. C., Impey, C. D., & Rix, H.-W. 2002, The Astronomical Journal, 124, 266, doi: 10.1086/340952

Peng, C. Y., Ho, L. C., Impey, C. D., & Rix, H.-W. 2010, The Astronomical Journal, 139, 2097, doi: 10.1088/0004-6256/139/6/2097

Perger, K., Fogasy, J., Frey, S., & Gabányi, K. A. 2025, Astronomy and Astrophysics, 693, L2, doi: 10.1051/0004-6361/202452422

Perrin, M. D., Sivaramakrishnan, A., Lajoie, C.-P., et al. 2014, Space Telescopes and Instrumentation 2014: Optical, Infrared, and Millimeter Wave, 9143, 91433X, doi: 10.1117/12.2056689

Popesso, P., Concas, A., Cresci, G., et al. 2023, Monthly Notices of the Royal Astronomical Society, 519, 1526, doi: 10.1093/mnras/stac3214

Pérez-González, P. G., Barro, G., Rieke, G. H., et al. 2024, The Astrophysical Journal, 968, 4, doi: 10.3847/1538-4357/ad38bb

Rieke, G. H., Alonso-Herrero, A., Weiner, B. J., et al. 2009, The Astrophysical Journal, Volume 692, Issue 1, pp. 556-573 (2009)., 692, 556, doi: 10.1088/0004-637X/692/1/556

Rieke, G. H., Buiten, V. A., Goldberg, C. E., et al. 2025, The Astrophysical Journal, 988, 17, doi: 10.3847/1538-4357/add2fd

Rieke, M. J., Robertson, B., Tacchella, S., et al. 2023, The Astrophysical Journal Supplement Series, 269, 16, doi: 10.3847/1538-4365/acf44d

Rinaldi, P., Bonaventura, N., Rieke, G. H., et al. 2024, doi: 10.48550/arXiv.2411.14383

Rujopakarn, W., Rieke, G. H., Weiner, B. J., et al. 2013, The Astrophysical Journal, 767, 73, doi: 10.1088/0004-637X/767/1/73

Satyapal, S., Vega, D., Heckman, T., O'Halloran, B., & Dudik, R. 2007, The Astrophysical Journal, 663, L9, doi: 10.1086/519995

Setton, D. J., Greene, J. E., de Graaff, A., et al. 2024, eprint arXiv:2411.03424, arXiv:2411.03424, doi: 10.48550/arXiv.2411.03424

Severgnini, P., Risaliti, G., Marconi, A., Maiolino, R., & Salvati, M. 2001, Astronomy and Astrophysics, 368, 44, doi: 10.1051/0004-6361:20000522

Shen, X., Hopkins, P. F., Faucher-Giguère, C.-A., et al. 2020, Monthly Notices of the Royal Astronomical Society, 495, 3252, doi: 10.1093/mnras/staa1381

Skelton, R. E., Whitaker, K. E., Momcheva, I. G., et al. 2014, The Astrophysical Journal Supplement Series, 214, 24, doi: 10.1088/0067-0049/214/2/24

Speagle, J. S., Steinhardt, C. L., Capak, P. L., & Silverman, J. D. 2014, The Astrophysical Journal Supplement Series, 214, 15, doi: 10.1088/0067-0049/214/2/15

Stepney, M., Banerji, M., Tang, S., et al. 2024, Monthly Notices of the Royal Astronomical Society, 533, 2948, doi: 10.1093/mnras/stae1970

Swinbank, A. M., Smail, I., Chapman, S. C., et al. 2004, The Astrophysical Journal, 617, 64, doi: 10.1086/425171

Tacchella, S., Lang, P., Carollo, C. M., et al. 2015, The Astrophysical Journal, 802, 101, doi: 10.1088/0004-637X/802/2/101

Taylor, M. 2022, 532, 3. https://ui.adsabs.harvard.edu/abs/2022ASPC..532....3T

team, T. p. d. 2024, Zenodo, doi: 10.5281/zenodo.13819579

Teplitz, H. I., Chary, R., Elbaz, D., et al. 2011, The Astronomical Journal, Volume 141, Issue 1, article id. 1, <NUMPAGES>16</NUMPAGES> pp. (2011)., 141, 1, doi: 10.1088/0004-6256/141/1/1

Toba, Y., Ueda, J., Lim, C.-F., et al. 2018, The Astrophysical Journal, 857, 31, doi: 10.3847/1538-4357/aab3cf

Tolman, R. C. 1930, Proceedings of the National Academy of Science, 16, 511, doi: 10.1073/pnas.16.7.511

Treu, T., & Koopmans, L. V. E. 2004, The Astrophysical Journal, 611, 739, doi: 10.1086/422245

Vulcani, B., Bamford, S. P., Häußler, B., et al. 2014, Monthly Notices of the Royal Astronomical Society, 441, 1340, doi: 10.1093/mnras/stu632

Wang, B., de Graaff, A., Davies, R. L., et al. 2024, doi: 10.48550/arXiv.2403.02304

Wang, B., de Graaff, A., Davies, R. L., et al. 2025a, The Astrophysical Journal, Volume 984, Issue 2, id.121, 21 pp., 984, 121, doi: 10.3847/1538-4357/adc1ca

Wang, B., Hennawi, J. F., Cai, Z., et al. 2025b, Monthly Notices of the Royal Astronomical Society, 539, 1562, doi: 10.1093/mnras/staf574

Whitaker, K. E., Ashas, M., Illingworth, G., et al. 2019, The Astrophysical Journal Supplement Series, 244, 16, doi: 10.3847/1538-4365/ab3853

Williams, C. C., Alberts, S., Ji, Z., et al. 2024, The Astrophysical Journal, 968, 34, doi: 10.3847/1538-4357/ad3f17

Wirth, G. D., Trump, J. R., Barro, G., et al. 2015, The Astronomical Journal, 150, 153, doi: 10.1088/0004-6256/150/5/153

Xue, Y. Q., Luo, B., Brandt, W. N., et al. 2016, The Astrophysical Journal Supplement Series, 224, 15, doi: 10.3847/0067-0049/224/2/15

Yaqoob, T. 2012, Monthly Notices of the Royal Astronomical Society, 423, 3360, doi: 10.1111/j.1365-2966.2012.21129.x

Yue, M., Eilers, A.-C., Ananna, T. T., et al. 2024, The Astrophysical Journal Letters, Volume 974, Issue 2, id.L26, 9 pp., 974, L26, doi: 10.3847/2041-8213/ad7eba

Zhang, H., Behroozi, P., Volonteri, M., et al. 2024, Monthly Notices of the Royal Astronomical Society, 529, 2777, doi: 10.1093/mnras/stae655

Zhang, J., Egami, E., Sun, F., et al. 2025, arXiv e-prints, arXiv:2505.02895, doi: 10.48550/arXiv.2505.02895

Zhuang, M., Li, J., & Shen, Y. 2023, JWST Proposal. Cycle 2, 3038. https://ui.adsabs.harvard.edu/abs/2023jwst.prop.3038Z/abstract

Zhuang, M.-Y., & Ho, L. C. 2023, Nature Astronomy, 7, 1376, doi: 10.1038/s41550-023-02051-4

Übler, H., Maiolino, R., Curtis-Lake, E., et al. 2023, Astronomy and Astrophysics, 677, A145, doi: 10.1051/0004-6361/202346137